Chapter

Group of Uniform Materials Based on Organic Salts (GUMBOS): A Review of Their Solid State Properties and Applications

Rocío L. Pérez, Caitlan E. Ayala and Isiah M. Warner

Abstract

Ionic liquids (ILs) are defined as organic salts with melting points below 100 °C. Such ionic compounds are typically formed using bulky cations and/or bulky anions in order to produce liquids or lower melting solids. ILs have been widely explored in several research areas including catalysis, remediation, solvents, separations, and many others. The utility of such compounds has also been recently broadened to include solid phase ionic materials. Thus, researchers have pushed the boundaries of ILs chemistry toward the solid state and have hypothesized that valuable properties of ILs can be preserved and fine-tuned to achieve comparable properties in the solid state. In addition, as with ILs, tunability of these solid-phase materials can be achieved through simple counterion metathesis reactions. These solid-state forms of ILs have been designated as a *g*roup of *u*niform *m*aterials *b*ased on *o*rganic *s*alts (GUMBOS). In contrast to ILs, these materials have an expanded melting point range of 25 to 250 °C. In this chapter, we focus on recent developments and studies from the literature that provide for fine tuning and enhancing properties through transformation and recycling of diverse ionic compounds such as dyes, antibiotics, and others into solid state ionic materials of greater utility.

Keywords: GUMBOS, solid-phase materials, nanoGUMBOS, fluorescence, sensors

1. Introduction

In recent years, many different kinds of materials and techniques have been developed for improved analytical measurements [1–7]. However, in order to be generally applicable, most materials should have several key properties. These desired properties include, but are not limited to (1) simplicity of preparation (e.g. development involves simply mixing two chemical solutions), (2) tunability (easy introduction of uniform multifunctionality through simple variations), and (3) limited or no toxicity (can be easily designed using materials that are already Food and Drug Administration (FDA) approved). As an example of the latter material, the near infrared (NIR) dye, indocyanine green, for near infrared fluorescence measurements has received early approval by the FDA [7].

On the basis of the above considerations, a wide variety of materials and nanomaterials have been developed and employed for bioanalytical and environmental

measurements. In regard to nanomaterials, studies reveal that in general primary properties such as spectra, colorimetric response, and magnetism are size dependent and somewhat tunable. Some of these materials, including carbon dots and silicon dots, exhibit very low cytotoxicities. However, other nanomaterials such as carbon nanotubes and quantum dots have considerably higher toxicities. In some cases, e.g. P-dots and nanogels [8–10], toxicity depends on the type of polymer used. Aqueous co-ordination complexes are another category of materials and nanomaterials with variable toxicities that have recently been used for analytical and environmental applications [11, 12].

We believe that when one does an exhaustive examination of the literature and considers the inherent properties identified above for improved analytical measurements, a logical conclusion is that ILs, GUMBOS, and nanomaterials derived from GUMBOS (nanoGUMBOS) represent novel classes of materials that best satisfies all of the above properties. Both ILs and GUMBOS are based on use of organic salts. Examples of typical ions used in these salts (ILs and GUMBOS) are shown in **Figure 1**.

These materials are continually being explored for improved analytical measurements. In fact, the literature on development of novel methodologies based on use of ionic liquids (ILs), a group of uniform materials based on organic salts (GUMBOS), and nanoGUMBOS is increasing at an ever-expanding rate. For example, numerous studies from the literature can be cited for utility of such materials in diverse areas such as antibiotics [13–15], cancer therapy [16–24], hydrogels [25, 26], cellular imaging [27, 28], chirality [29–33], dye-sensitized solar cells (DSSCs) [34–36], extractions [37–39], gel electrophoresis [40, 41], detection of reactive oxygen species [42], liquid crystals [43], mass spectrometry [44], nanomaterials [45–52], optoelectronics [53–56], sensors [57–61], separation science [62, 63], spectroscopy [64–67], volatile organic compounds (VOCs) [68–75], as well as a number of patents and patent applications [76–78]. **Figure 2** provides an abbreviated summary of numerous applications of ILs and GUMBOS.

We note that GUMBOS and nanoGUMBOS are solid phase organic salts (m.p. > 25 °C and < 250 °C) and ILs are typically liquids or low melting solids (m.p. < 100 °C). See **Figure 3** below for differentiation between ILs and GUMBOS in terms of melting points. Therefore, some GUMBOS (and nanoGUMBOS) materials fit into the general category of frozen ILs since ILs from 100 °C down to 25 °C are solids. However, many GUMBOS materials are outside the generally accepted temperature range for ILs. Accordingly, a new, more general term of GUMBOS, as defined above, was adopted to apply to this entire class of solid phase organic salts.

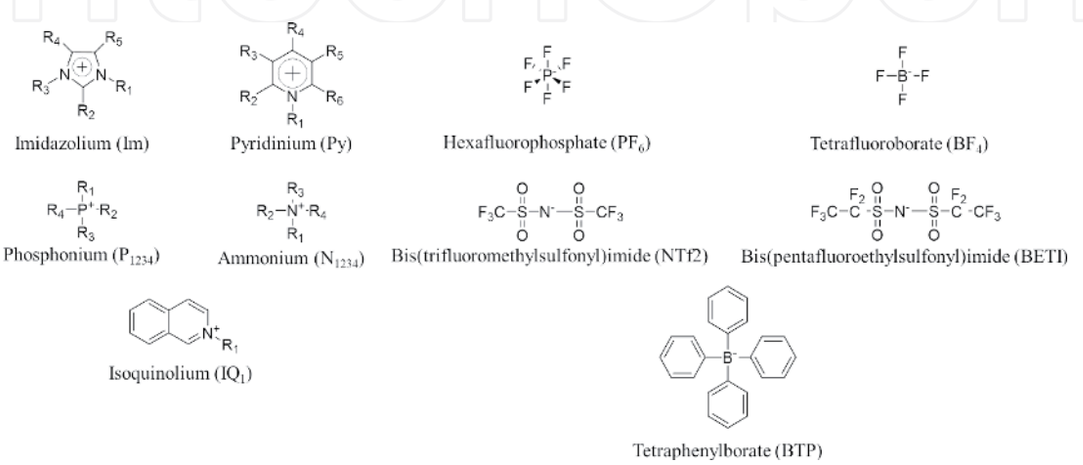

Figure 1.
Typical cations and anions used for ILs/GUMBOS production.

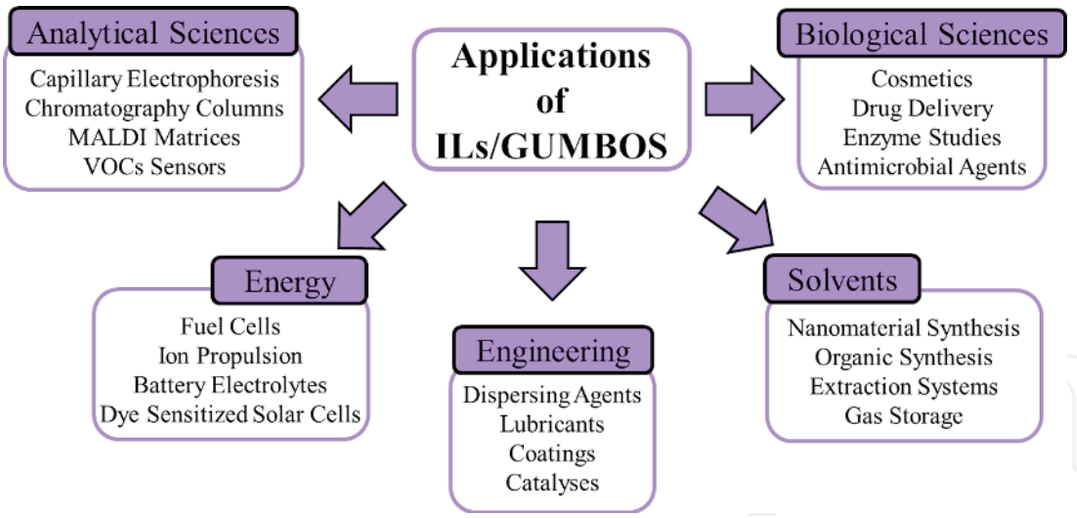

Figure 2.
Applications of ILs/GUMBOS in different research areas.

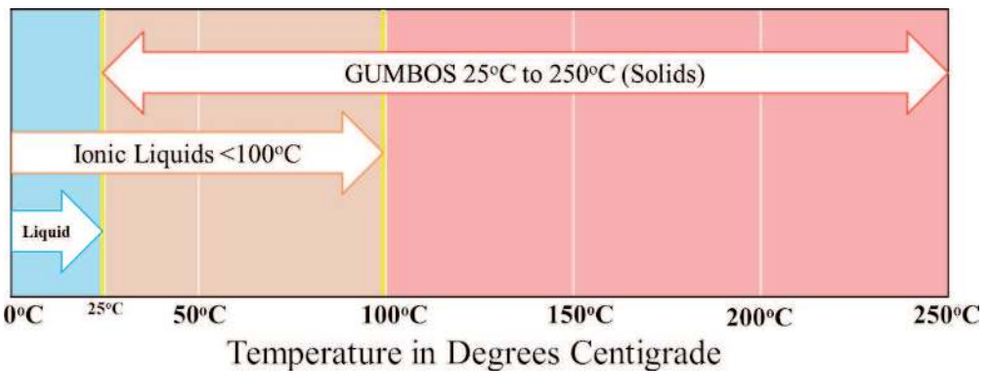

Figure 3.
Melting points range of ILs and GUMBOS.

To date, numerous strategies for this kind of chemistry have been developed. In this chapter, we desire to discuss some of these applications in detail, particularly as applied to the general area of analytical and environmental chemistry.

2. Biological applications

ILs have been recognized for their properties such as non-volatility, viscosity, negligible vapor pressure, high ionic strength, thermal stability, and low toxicity, among others [79]. As a result of these important properties, ILs were initially designated as green and designer solvents (i.e. first generation ILs) [80]. Eventually, due to their high tunability, new ILs were strategically designed for a variety of functional materials, including lubricants, catalysts, energy materials, etc. [81–86]. These types of ILs are known as second generation ILs. Finally, major interest has focused on development of new ILs (third generation ILs) for biological applications to achieve biocompatible and low toxic compounds through use of bio-counterions [87, 88]. Moving forward, more attention from the scientific community has focused on development, or recycling of, various molecules into solid phase materials (frozen ILs or GUMBOS) for several biological applications [17, 89–91]. In this section, the use of frozen ILs and GUMBOS for biological applications such as cancer and antibiotic therapies are discussed.

2.1 GUMBOS and nanoGUMBOS as chemotherapeutic agents

Cancer is the second leading cause of death in the United States and is a major health concern worldwide [92]. Treatment of cancer typically includes surgery, radiotherapy, hormone therapy, immunotherapy and/or chemotherapy [93]. Effectiveness of these treatments depends upon several factors, such as stage of cancer at the moment of diagnosis, general health of the individual, size and type of tumor, among others. In general, treatment of a person with cancer will involve a combination of therapies as a result of these several factors, and chemotherapy is the most commonly employed treatment. Unfortunately, chemotherapy will often be accompanied with several adverse effects, such as nausea, vomiting, diarrhea, fatigue, malnutrition, anemia, hepatotoxicity, nephrotoxicity, among others [94–96]. These side effects are the result of high toxicity of typical chemotherapeutic agents that generally lack selectivity toward carcinogenic cells. For all of these reasons, over the past decades major attention has focused on developing new chemotherapeutic agents that are selectively toxic to cancer cells [97–99]. Moreover, investigations have also focused on early detection methods that involve use of tumor-targeting dyes, as well as near infrared (NIR) dyes for detection, photothermal therapy (PTT) and photodynamic therapy (PDT) [100–103].

Due to their relatively high division rate and subsequent growth relative to normal cells, cancer cells use more energy [104–106]. It is well established that the mitochondria are organelles that synthesize adenosine triphosphate (ATP), which is the energy source of cells. As a result, mitochondria in tumor cells have a higher negative mitochondrial membrane potential as compared to normal cells. For this reason, major interest has been directed toward study of cationic compounds as well as positively charged vesicles as chemotherapeutic agents. Several publications from the literature document that these type of compounds are attracted to, and accumulate more selectively, in this organelle of cancer cells, resulting in disruption of ATP synthesis and subsequent induction of cell death [16, 17, 22, 89, 107, 108].

Cationic rhodamine dyes have been studied as mitochondrial targeting agents as early as the 1970s [109–114]. Furthermore, studies with rhodamine dyes demonstrate that these dyes are toxic to cells above certain concentrations [115, 116]. In contrast, it has been previously reported that hydrophobicity of drugs may improve cellular uptake and distribution inside cancer cells [117]. For this reason, Magut et al. hypothesized that counterion variation in rhodamine 6G dye ($[R6G]^+$) may tune its hydrophobicity [22]. In this regard, four anions: ascorbate ($[Asc]^-$), trifluoremethanesulfonate ($[OTf]^-$), tetraphenylborate ($[TPB]^-$) and bis(perfluoroethylsulfonyl)imide ($[BETI]^-$) were employed to synthesize, through a simple metathesis reaction, four R6G-based GUMBOS. Relative hydrophobicities for each GUMBOS were determined, and the following trend in increasing hydrophobicity from [R6G][Asc] < [R6G][OTf] < [R6G][TPB] < [R6G][BETI] was observed in this study. Clearly, anion variation affected and tuned hydrophobicity, along with other physico-chemical properties, of the parent dye. The low water solubility of these compounds allowed synthesis of nanoGUMBOS through a simple reprecipitation method. *In vitro* cellular cytotoxicity of these GUMBOS and nanoGUMBOS towards normal breast cells (Hs578T), hormone-independent human breast adenocarcinoma (MDA-MB-231) and hormone-dependent human breast adenocarcinoma (MCF7) cell lines using an MTT assay was evaluated. Interestingly, evaluation of results obtained for [R6G][Asc] and [R6G][OTf] showed that these GUMBOS were highly toxicity toward both normal and cancer cell lines. Similar behavior was observed with the parent compound, [R6G][Cl]. This trend was explained through similar water solubilities of these compounds. In contrast, cytotoxicity results obtained for [R6G][BETI] and [R6G][TPB] indicated

that these compounds were more selectively toxic toward cancer cell lines than normal cells. Moreover, these GUMBOS were more toxic against MDA-MB-231 cancer cells, which were the most aggressive cancer cell lines evaluated using 50% inhibition concentration (IC_{50}) values of 11.4 and 12.2 μM for [R6G][BETI] and [R6G][TPB], respectively. Additionally, confocal microscopy studies demonstrated that these nanoGUMBOS were localized inside the mitochondria of cancer cells, which resulted in decreased synthesis of ATP.

Following this study, other researchers focused on evaluating the mechanism of action and internalization of [R6G][BETI] nanoGUMBOS in cells [18]. In that study, Bhattarai and coworkers performed a series of *in vitro* experiments at different incubation temperatures, in the presence of several endocytic inhibitors, as well as in depletion media, to study internalization of [R6G][BETI] nanoGUMBOS. These experiments allowed the investigators to conclude that these nanoGUMBOS were internalized into cancer cells through a clathrin mediated endocytosis pathway. In contrast, these nanoGUMBOS were found to be internalized in normal cells through an independent endocytic route. Interestingly, it was further demonstrated that [R6G][BETI] nanoGUMBOS passed through lysosome vesicles before reaching the mitochondria. For this reason, Bhattarai and coworkers investigated the integrity of these nanoparticles at lysosomic pH (pH = 4) and normal pH (7.4) values using transmission electron microscopy (TEM) and dynamic light scattering (DLS) experiments. Evaluation of these results demonstrated that nanoparticles lost integrity under acidic pH similar to those in the lysosome, thus releasing $[R6G]^+$ that subsequently entered the mitochondria, and inhibited ATP synthesis and eventually causing apoptosis of cancer cells. Internalization in normal cells did not involve entry through the lysosome. Thus, these investigators concluded that this differential internalization route was the primary reason for selectivity of [R6G][BETI] nanoGUMBOS towards cancer cells. Finally, Bhattarai and co-workers evaluated *in vivo* efficacy of nanoGUMBOS in tumor size reduction in an athymic nude mouse model. Evaluation of these results demonstrated that nanoGUMBOS inhibited tumor growth and decreased tumors size by 50% making this material a good candidate for *in vivo* chemotherapeutic applications [18].

It has been previously reported in the literature that there is a strong correlation between size, hydrophobicity, and surface charge of nanomaterials as related to resultant toxicity against cancer cells [118, 119]. Moreover, *in vivo* studies have demonstrated that nanoparticle size has an important effect in increasing cellular uptake into tumor tissue via leaky tumor vasculature through a phenomenon known as enhanced permeability and retention (EPR) effect [120]. In this regard, Hamdan et al. have shown that use of cyclodextrins (CDs) in nanoGUMBOS synthesis results in more uniform and smaller nanoparticles [45]. CDs are cyclic oligosaccharides having conical shapes, with an inner hydrophobic cavity and an external hydrophilic surface. This characteristic structure of CDs allows interaction with some hydrophobic compounds to provide encapsulation and increased water solubility [121, 122]. For this reason, Bhattarai et al. investigated the synthetic procedure of [R6G][BETI] and [R6G][TPB] nanoGUMBOS in the presence of three different CDs: 2-hydroxypropyl-αCD (HP-αCD), 2-hydropropyl-βCD (HP-βCD), and γ-CD in order to optimize nanoparticle size, uniformity and stability [17]. In this report, nanoparticle synthesis was performed by directly mixing stoichiometric quantities of each parent compound in the presence of predetermined concentrations of each CD until synthetic conditions were optimized. These researchers noticed, from TEM and zeta potential data, that CD-templated nanoparticles presented lower size and higher zeta potentials as compared to control nanoGUMBOS (**Figure 4**). In **Table 1**, size, zeta potential and cytotoxicity of CD-templated and control nanoGUMBOS are summarized. Based on evaluation of results obtained

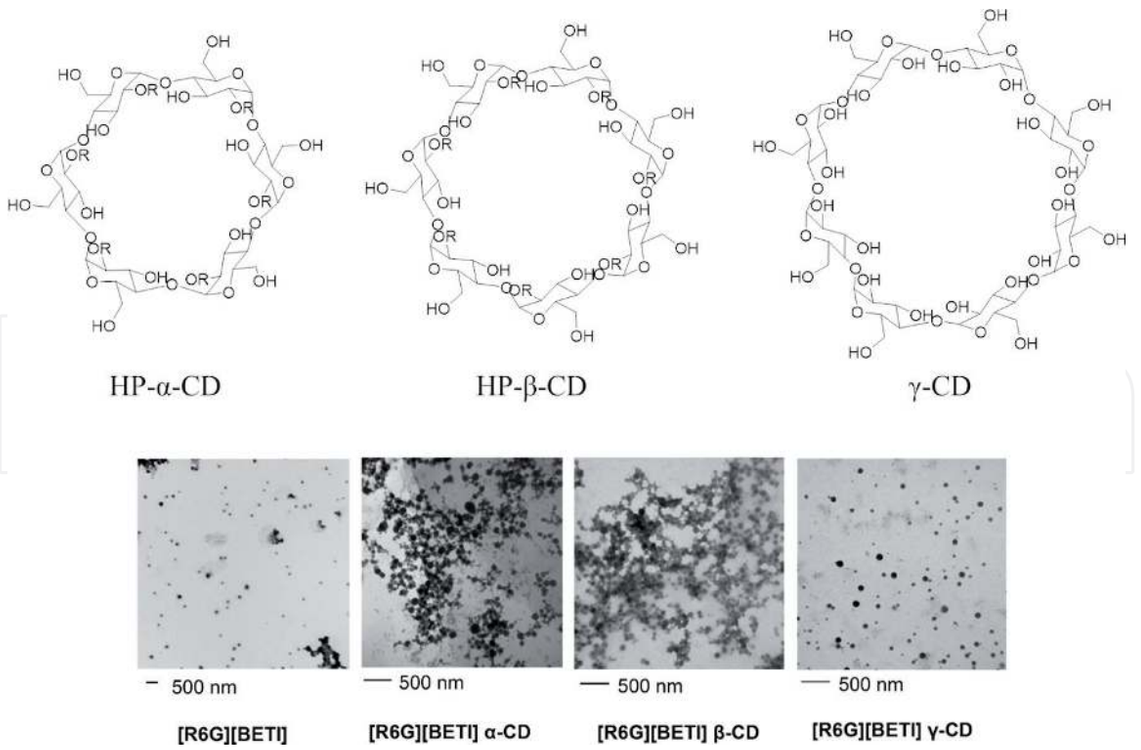

Figure 4.
CDs structures and TEM images of [R6G][BETI] nanoGUMBOS in absence and presence of CDs.

Compound	Size (nm)	Zeta potential (mV)	IC_{50} MDA-MB-231 ($\mu g\ mL^{-1}$)	IC_{50} MiaPaca ($\mu g\ mL^{-1}$)
[R6G][TPB] control	105 ± 16	−23.1 ± 1.2	7.3 ± 1.1	0.75 ± 0.05
[R6G][TPB] HP-α-CD	55 ± 6	−27.2 ± 1.5	2.6 ± 0.2	0.37 ± 0.03
[R6G][TPB] HP-β-CD	44 ± 4	−29.5 ± 1.1	2.7 ± 0.3	0.39 ± 0.06
[R6G][TPB] γ-CD	69 ± 6	−28.3 ± 0.9	1.4 ± 0.3	0.24 ± 0.04
[R6G][BETI] control	99 ± 12	−24.3 ± 1.2	4.2 ± 0.4	0.45 ± 0.05
[R6G][BETI] HP-α-CD	68 ± 8	−29.0 ± 1.1	1.6 ± 0.3	0.24 ± 0.03
[R6G][BETI] HP-β-CD	66 ± 4	−30.1 ± 0.8	1.7 ± 0.2	0.26 ± 0.04
[R6G][BETI] γ-CD	80 ± 5	−29.8 ± 1.6	2.3 ± 0.4	0.30 ± 0.03

Table 1.
Size, zeta potential, IC_{50} for MDA-MB-231 and MiaPaca cell lines for parent and CD-templated nanoGUMBOS [17].

using cytotoxicity studies performed with MDA-MB-231 and pancreatic cancer (MiaPaca) cell lines, these researchers noticed a significant decrease in IC_{50} values, suggesting that CD-templating enhances toxicity of these nanoparticles.

Another approach from this laboratory involved use of an IR-780 dye to synthesize GUMBOS and nanoGUMBOS [16]. IR-780 is a NIR fluorescent dye that has been studied as a possible theranostic agent since it can be employed as an imaging agent as well as a photothermal and photodynamic agent [123–125]. In this regard, Chen et al. synthesized three IR-780-based GUMBOS through a simple metathesis

reaction [16]. Anions evaluated in that study were $[Asc]^-$, $[OTf]^-$, and $[BETI]^-$. Relative hydrophobicity and spectroscopic properties of these GUMBOS were evaluated and compared to the parent compound [IR-780][I]. These researchers found the following hydrophobicity trend: [IR-780][BETI] > [IR-780][I] > [IR-780][OTf] > [IR-780][Asc]. As a result of these larger hydrophobicity values, nanoGUMBOS synthesis was performed through a simple reprecipitation method. Cytotoxicity of [IR-780][BETI] nanoGUMBOS and [IR-780][I] nanomaterials were studied *in vitro* in three different cancer cell lines: MDA-MB-231, MCF7 and MiaPaca using an MTT assay, and IC_{50} values were calculated. Interestingly, IC_{50} for [IR-780][BETI] were lower than IC_{50} values for nanoparticles of the parent compound for all cell lines evaluated. Furthermore, this [IR-780][BETI] nanoGUMBOS presented the lowest IC_{50} values against MDA-MB-231, which was the most invasive and aggressive cancer cell line evaluated. These findings indicate that a simple anion variation in a parent compound can selectively change its cytotoxicity towards cancer cell lines.

Relative cell viability was evaluated for each nanoGUMBOS in normal breast cells. These researchers found that all nanoGUMBOS studied were more selectively cytotoxic against cancer cell lines. Results observed after cellular uptake and fluorescence microscopy studies of each nanomaterial allowed these researchers to conclude that nanoGUMBOS, especially [IR-780][BETI], were internalized and accumulated within the mitochondria in higher amounts than with the parent compound. It has been previously reported in the literature that mitochondrial accumulation of [IR-780][I] is followed by cellular apoptosis [126]. In addition, these researchers investigated nanoGUMBOS as inducers of necrosis or mitochondrial disruptors, by employing a mitochondrial toxicity assay. Evaluation of these results showed that nanoGUMBOS presented behavior similar to [IR-780][I] nanomaterials and acted as mitochondrial toxins by inhibiting oxidative phosphorylation. In summary, nanoGUMBOS synthesized in this work represented great potential as possible chemotherapeutic agents along with a strategic advantage as compared to other reported nanomaterials that require complicated synthetic procedures and labels to increase selectivity against cancer cells [127–130].

In another work, Chen and coworkers evaluated *in vitro* and *in vivo* cytotoxicity and photothermal properties of CD-[IR-780][TPB] complexed nanoGUMBOS [89]. In this work, [IR-780][TPB] GUMBOS were synthesized and nanoGUMBOS were obtained in using HP-β-CD. In this case, CD-[IR-780][TPB] nanoGUMBOS represented larger diameters than nanoGUMBOS without CD (**Figure 5a** and **b**). These results were different from those obtained by Bhattarai et al. [17], in which CDs acted as a template. Based on analyses of TEM and differential scanning calorimetry results, along with computational modelling, the authors demonstrated that a stable complex was formed between HP-β-CD and [IR-780][TPB]. Afterwards, these researchers performed relative cell viability studies in breast cancer cell lines (MDa-MB-231, MCF-7, and Hs578T) and normal breast cell lines (Hs578Bst and HMEC). Based on these results, Chen and partners demonstrated that CD-[IR-780][TPB] nanoGUMBOS were more selective against cancer cells in comparison to [IR-780][I] nanoparticles and [IR-780][TPB] nanoGUMBOS. Moreover, CD-[IR-780][TPB] nanoGUMBOS were not toxic to breast normal cells in the concentration range evaluated.

Additionally, cell viability of CD-[IR-780][TPB] nanoGUMBOS were evaluated using MDA-MB-231 and Hs578T cell lines with NIR laser irradiation (808 nm). This resulted in a further decrease in IC_{50} values for these nanomaterials. Furthermore, these results demonstrate that CD-[IR-780][TPB] nanoGUMBOS represent highly potent chemo- and photothermal therapeutic agents. Finally, Chen et al. also evaluated *in vivo* efficacy and PTT activity of nanoGUMBOS and

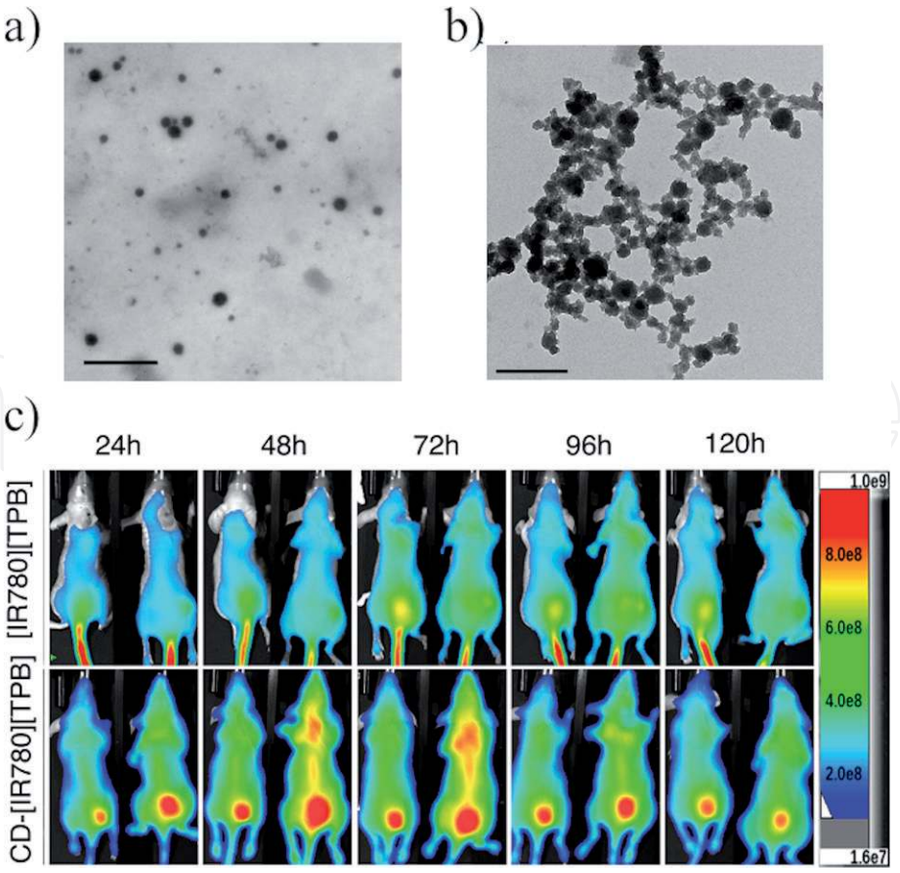

Figure 5.
TEM images of (a) [IR-780][TPB] nanoGUMBOS, (b) CD-[IR-780][TPB] nanoGUMBOS (scale bar represents 500 nm). (c) In vivo fluorescence of [IR-780][TPB] and CD-[IR-780][TPB] nanoGUMBOS at different time points.

CD-nanoGUMBOS using an MDA-MB-231 tumor xenograft model. Interestingly, NIR fluorescence intensity of mice demonstrated that CD-nanoGUMBOS distributed more rapidly and provided a higher tumor accumulation than nanoGUMBOS (**Figure 5c**). Moreover, these authors observed tumor decrease in mice treated with CD-[IR-780][TPB] nanoGUMBOS plus irradiation. Thus, these results indicated that CD-nanoGUMBOS have great potential as chemo-theranostic agents.

Broadwater et al. combined heptamethine cyanine cation ($[Cy]^+$) with several anions, such as iodide ($[I]^-$), hexafluoroantimonate ($[SbF6]^-$), and hexafluorophosphate ($[PF6]^-$), o-carborane ($[CB]^-$), along with bulkier anions such as tetrakis(4-fluorophenyl)borate ($[FPhB]^-$), cobalticarborane ($[CoCB]^-$), tetrakis (pentafluorophenyl) borate ($[TPFB]^-$), tetrakis[3,5-bis(trifluoro methyl)phenyl] borate ($[TFM]^-$), and Δ-tris(tetrachloro-1,2-benzene diolato) phosphate(V) ($[TRIS]^-$) to obtain several Cy-based organic salts [131]. Redox values, zeta potentials, HOMO energy level, as well as optical properties of all [Cy]-based organic salts were determined in that study. These results demonstrated that counterion exchange allowed tuning of HOMO energy levels of $[Cy]^+$. However, absorbance of all synthesized Cy-based organic salts spectra remained essentially the same.

The above cited authors then synthesized nanoparticles through a simple reprecipitation method. All Cy-based organic salts nanoparticles were determined to have an average size between 5–9 nm and were stable for 22 days. Following these experiments, Broadwater and collaborators evaluated cytotoxicity and phototoxicity of Cy-based organic salt nanoparticles against two different cell lines: human lung carcinoma (A549) and metastatic human melanoma (WM1158) in the absence and presence of 850 nm light. These results indicated that $[I]^-$, $[SbF6]^-$, and

$[PF6]^-$, $[CB]^-$ presented high cytotoxicity under both condition evaluated, making these compounds good candidates as chemotherapeutic agents. When $[Cy]^+$ was paired with $[FPhB]^-$ and $[CoCB]^-$ anions, nanoparticles of these compounds were determined to be slightly toxic at concentrations of 7.5 μM without NIR irradiation. However, when these compounds were irradiated with NIR laser, they were highly toxic at 5.5 μM concentrations, which indicates that [Cy][FPhB] and [Cy][CoCB] presented high potential as phototoxic agents. In contrast, compounds where $[Cy]^+$ was combined with bulky anions: $[TPFB]^-$, $[TFM]^-$, and $[TRIS]^-$ showed non-cytotoxicity against lung cancer cells. As a result, Broadwater, et al. concluded that these compounds could be employed as imaging agents. Based on cytotoxicity studies, the authors proved that toxicity of $[Cy]^+$ dye was tuned through counterion exchange. Finally, these authors evaluated *in vitro* imaging properties of all Cy-based organic salts nanoparticles. Analyses of these results demonstrated that non-toxic Cy-based organic salts could be employed at higher concentrations that resulted in a higher fluorescence intensity. Additionally, an *in vivo* evaluation of these compounds demonstrated that these compounds were accumulated in tumor sites.

2.2 Recycling of antimicrobial agents and other medicines

Antibiotics were introduced into modern medical practices in the 19th century with the discovery of sulfonamides in the 1930s and penicillin in the 1940s [132–134]. Without such medication, people often died from infections such as syphilis, gonorrhea, and pneumonia. Thus, use of these antibiotics represented the saving of many thousands of lives and a new era in medicine [135, 136]. Nevertheless, over the years since such discoveries, increased production, indiscriminate use, and over consumption of antibiotics has created an unfortunate outcome of antibiotic and multi-antibiotic resistant bacteria [137–139]. For this reason, the scientific community has begun to focus on syntheses of new antibiotics that could provide alternative therapies in order to avoid bacterial resistance mechanisms. However, syntheses of completely new antibiotics require great ingenuity, intense synthetic prowess, excellent purification, and considerable resources [140–142]. As an alternative to the foregoing strategy, several research groups have applied an ion metathesis strategy for antibiotic renewal and enhancement. Thus, recycling of current antibiotics have become a reality.

Florindo et al. synthesized ampicillin based ILs employing triethylammonium ($[TEA]^+$), choline ($[N_{1112}OH]^+$), trihexyltetradecylphosphium ($[P_{66614}]^+$), 1-ethyl-3-methylimidazolium $[C_2MIm]^+$, 1-hydroxy-ethyl-3-methylimidazolium $[C_2OHMIm]^+$ and cetylpyridinium $[C_{16}Pyr]^+$ as cations to tune crystalline forms and pharmaceutical properties [143]. In that study, water solubility, octanol/water partition coefficient ($K_{o/w}$), and phospholipid/water partition (K_p) of synthesized compounds were evaluated. Water solubility of active pharmaceutical ingredients (API) is of great importance because it determines the accessibility and distribution of API within the body. Using water solubility results at room temperature and at 37 °C, the following trend was observed: $[C_2OHMIM][Amp] > [N_{1112}OH][Amp] > [C_2MIM][Amp] > [TEA][Amp]$. All Amp-based ILs studied showed lower solubility as compared to [Na][Amp] at room temperature. However, cations with hydroxyl groups presented higher solubility at 37 °C than the parent compound. In contrast, Amp-ILs with longer carbon chains, such as $[P_{66614}]^+$ and $[C_{16}Pyr]^+$, showed K_p values higher than the parent compound, indicating that these compounds could interact better with cellular membranes. Based on results obtained in this study, $[N_{1112}OH][Amp]$ provided the most promising pharmaceutical properties with higher solubility, lower cytotoxicity, lower inflammation response and similar $K_{o/w}$ relative to the parent compound. Thus, these researchers confirmed

that pharmaceutical properties from [Na][Amp] could be finely tuned through simple counterion exchanges.

In another study, the same researchers synthesized ciprofloxacin and norfloxacin fluoroquinolones (FQ) based protic ionic liquids (PILs) through reaction with mesylic acid ([Mes][H]), gluconic acid ([Glu][H]), and glycolic acid ([Gly][H]) to tune their crystalline forms and pharmaceutical properties to enhance their bioavailability [144]. In this case, similar properties as in previous studies were evaluated [143]. The authors observed a clearly increasing trend in aqueous solubility depending on the anion present in FQ-PILs: $[Gly]^-$ < $[Mes]^-$ < $[Glu]^-$. These observations were in agreement with $K_{o/w}$ studies obtained by these researchers. Similar K_p results for parent FQs were obtained for their respective organic salts, which indicated that interactions with cellular membranes were not affected. Based on these results, Florindo et al. concluded that FQ-based organic salts studied in this work presented high potential as alternatives to the original antibiotics.

Santos, et al. employed two FQs (ciprofloxacin and norfloxacin) to synthesize active pharmaceutical ingredient (API)-based ILs by combining their salts with the following cations: $[N_{1112}OH]^+$, $[C_{16}Pyr]^+$, 1-ethyl-3-methylimidazolium $[C_2MIm]^+$, 1-hydroxy-ethyl-3-methylimidazolium $[C_2OHMIM]^+$, 1-(2-hydroxyethyl)-2,3-dimethylimidazolium $[C_2OHDMIm]^+$, and 1-(2-methoxyethyl)-3-methylimidazolium ($[C_3OMIm]^+$) [145]. Water solubility of the synthesized compounds were evaluated, and the following trend was observed: $[EMIM]^+$ < $[Ch]^+$ < $[C_2OHDMIM]^+$ ≈ $[C_3OMIM]^+$ < $[C_2OHMIM]^+$. This trend was similar to results reported in a previous study from the same group [145]. The authors determined IC_{50} concentrations of these FQ-ILs in this study against three bacteria: *Bacillus subtilis* (*B. subtilis*), *Staphylococcus aureus* (*S. aureus*) and *Klebsiella pneumoniae* (*K. pneumonia*) and compared results with IC_{50} values of the parent compounds. In order to evaluate if the synthesized compounds were more effective than the parent compounds, these researchers calculated the relative decrease of inhibitory concentration (RDIC) obtained by divided the minimum inhibitory concentration (MIC) values of each API-ILs by MIC of the corresponding API. Interestingly, most compounds evaluated in this work presented better antimicrobial activity than the original FQ with RDIC values higher than one [145].

Frizzo et al. employed sodium ibuprofen ([Na][Ibu]) and sodium docusate to synthesize API-based ILs [146]. Sodium cations in the parent compounds were replaced with ranitidine ($[Ran]^+$), diphenhydramine, glycine, or glycine ethyl cations. In this work, these researchers tested all synthesized compounds along with parent compounds against several types of bacteria and species of *Candidas* fungus. Evaluation of their results demonstrated that, in general, all API-ILs presented better antifungal activity than the precursors. For example, all ibuprofen-based ILs demonstrated antifungal activity. Interestingly, [Ran][Ibu] ILs presented antifungal activity when the parent compounds did not. In contrast, most API-ILs presented higher antibacterial activity than the parent compounds. These researchers synthesized ibuprofen- and docusate- based ILs that demonstrated high potential as antimicrobial and antifungal agents.

Ferraz et al. [147] also employed amoxicillin ($[seco\text{-}Amx]^-$) and penicillin G ($[seco\text{-}Pen]^-$) in combination with imidazolium, choline, ammonium, phosphonium and pyridinium cations to synthesize antibiotic based API-ILs. Resistant and sensitive Gram positive and Gram negative bacteria, including methicillin resistant *S. aureus* (MRSA ATCC 43300), were employed to test antimicrobial efficacy of these API-ILs through use of a broth micro dilution method. Evaluation of results obtained on sensitive strains demonstrated that only three of all evaluated compounds $[C_2OHMIM][seco\text{-}Amx]$, $[C_2OHMIM][seco\text{-}Pen]$, and [TEA][seco-Pen], produced lower or equal MIC values than the parent compounds and RDIC values

equal to or higher than one. However, more interesting results were obtained when these compounds were tested against resistant bacteria such as *Escherichia coli* (*E. coli*) strains CTX M9 and CTX M2 as well as methicillin-resistant *S. aureus* ATCC 43,300. When tested against resistant *E. coli*, $[C_{16}Pyr][seco\text{-}Amx]$ presented the highest RDIC value (> 100). In contrast, $[C_{16}Pyr][seco\text{-}Amx]$ and $[C_{16}Pyr][seco\text{-}Pen]$ were more effective against *S. aureus* ATCC 43,300 with RDICs higher than 1000 and 100, respectively. Another compound that was more effective than the commercial antibiotic was $[N_{1112}OH][seco\text{-}Pen]$ with RDIC larger than 5. These findings clearly demonstrate that $[C_{16}Pyr]^+$ cation played an important role in antimicrobial activity of synthesized API-ILs acting in a synergetic way along with API present in the compound [147].

Cole and coworkers proposed recycling of antibiotics into GUMBOS [15]. In this work, ampicillin based GUMBOS (Amp-GUMBOS) were synthesized through a simple metathesis reaction where a sodium cation was replaced by hexadecyl-methyl-imidazolium ($[C_{16}MIm]^+$), hexadecyl-dimethyl-imidazolium ($[C_{16}M_2Im]^+$) and $[C_{16}Pyr]^+$. These Amp-ILs were tested against Gram negative and positive bacteria and compared to parent compounds. Interestingly, MIC values obtained for Amp-GUMBOS in these experiments demonstrated that these concentrations were between 2 to 43 times lower than MIC values determined for ampicillin.

Following their previous studies, Cole and co-workers employed chlorhexidine and ampicillin to synthesize antibacterial GUMBOS [14]. These two antibacterial agents are commonly used in veterinary practices to treat and/or prevent the presence of *E. coli* strains that are commonly found in cattle. The presence of *E. coli* strains could produce severe illness in humans, especially *E. coli* O157:H7, which is well-known because it produces bloody diarrhea, haemorrhagic colitis and haemolytic uraemic syndrome in humans [148–150]. For this reason, development of a prophylactic treatment for this type of bacteria are highly desirable for eradication or minimization in cattle to prevent human illnesses. Cole et al. evaluated the efficacy of this Chlorhexidine di-ampicillin GUMBOS to kill several *E. coli* O157:H7 strains isolated from different sources such as chicken, pork, beef, apple cider, burger and humans [14]. Chlorhexidine di-ampicillin GUMBOS was found to kill *E. coli* strains more effectively since these GUMBOS presented MIC values much lower than the parent compounds and their unreacted stoichiometric mixture. Moreover, interaction indices indicated that this antimicrobial GUMBOS presented a synergetic mechanism effect. Chlorhexidine is a commonly used antiseptic; however, it presents high cytotoxicity against normal cells. For this reason, these researchers studied cytotoxicity of GUMBOS, parent compounds and unreacted stoichiometric mixtures in Hela cells. Interestingly, GUMBOS were less toxic than parent chlorhexidine, reaching 93% cell viability.

In another work, Cole and coworkers recycled four β-lactam antibiotics (ampicillin, cephalothin, carbenicillin and oxicilin) into GUMBOS, by combining them with chlorhexidine diacetate [151]. Twenty-five bacteria isolates were obtained from several sources, where most of these were resistant or multi-resistant to antibiotics. These four β-lactam – based chlorhexidine GUMBOS were tested against these isolates. Results obtained by Cole and coworkers demonstrated that these β-lactam – based chlorhexidine GUMBOS were more effective against these isolates with MIC values in a range between 0.1 to 32 μM as compared to parent compounds with higher MIC (5 to >1250 μM). Moreover, in this report Cole et al. evaluated if these GUMBOS presented a synergetic, additive or antagonist effect relative to their unreacted mixtures of stoichiometric equivalents. Interestingly, these researchers found that for most GUMBOS studied, the observed effect was synergetic [152].

Neisseria gonorrhoeae is another bacterial target that is primarily sexually transmitted and responsible for the disease gonorrhea [153]. In recent years,

N. gonorrhoeae resistance to current treatments have been isolated and reported around the world [154, 155]. Lopez et al. have synthesized GUMBOS from an antiseptic octenidine and a discontinued antibiotic carbenicillin as a possible alternative to reduce and minimize *N. gonorrhoeae* transmission [156]. The zone of inhibition (ZOI) for *N. gonorrhoeae* strains and clinical isolates were studied in the presence of GUMBOS, parent compounds, and antibiotics currently employed for gonorrhea treatment. Evaluation of results obtained demonstrated that synthesized GUMBOS presented an additive effect as compared to the parent compounds as well as an equivalent antimicrobial activity like azithromycin.

3. Sensing materials

Sensing strategies for a variety of systems, from biological targets [157], environmental and regulatory applications [158, 159], mechanical integrity of structures [160–162], and more [60, 163], are continuously under investigation in the scientific community. In general, recognition can be categorized into two different methodologies: targeted and non-targeted [164]. Targeted strategies require materials that are designed to respond to specific analyte(s) and thus, require a high degree of specificity for singular analytes [63, 159, 165]. Differential strategies, however, can potentially provide information within convoluted and complex mixtures based on several non-specific sensors or one sensor with multi-layered responses to different analytes [166]. In the following sections, solid-state ionic materials for various sensing applications are discussed.

3.1 Ratiometric sensing: fluorescence imaging

Previous investigations using fluorescent imaging with solid-state ionic materials have undergone scrutiny to prevent or reduce self-quenching between dye molecules in order to enhance properties such as excitation energy transfer and achieve on/off switching in nanoparticle structures [167–172]. Traditionally, dye self-quenching has been rectified by introducing bulky side-chains into the molecular structure via synthetic organic chemistry [172–174]. However, this type of strategy requires several synthetic and purification steps that result in increased expense. In contrast, large counterions were observed to also inhibit this self-quenching phenomenon in a much more facile manner through a simple ion metathesis reaction [28, 50]. Several research groups have capitalized on this strategy to study polymeric nanoparticle encapsulated rhodamine-derived GUMBOS, respective photophysical properties, and cellular uptake ability for imaging applications along with targeting agents to provide organelle contrast [28, 172, 175, 176].

More recently, researchers have diversified beyond cellular imaging techniques. For example, Severi et al. have explored polymer encapsulation of nanoprobes that undergo efficient Förster resonance energy transfer (FRET) for potential point-of-care applications with smartphones [177]. In this study, ester-modified cations rhodamine 110 and 6G cations ($[R110]^+$ and $[R6G]^+$, respectively) were employed as FRET donor dyes with bulky tetrakis[3,5-bis(1,1,1,3,3,3-hexafluoro-2-methoxy-2-propyl)phenyl]borate trihydrate ($[F12]^-$) and tetrakis(perfluoro-tertbutoxy) aluminate ($[F9\text{-}Al^-]$) counterions [176]. These Ion pairs were encapsulated with DNA cancer marker (survivin) targeted polymer nanoparticles, which were also functionalized using a red-emitting oligonucleotide-functionalized dye as a FRET acceptor. After nanoparticle size, quantum yield (QY), FRET acceptor concentration optimization, and evaluation of FRET capabilities, encapsulated [R6G][F9-Al] nanoprobes were evaluated for red, green, blue (RGB) survivin DNA marker

detection in solution using fluorescence spectroscopy. These researchers found that their designed system had a limit of detection of 3pM. Upon optimization of microscopic and digital imaging, these researchers also found that using an iPhone SE, [R6G][F9-Al] as an encapsulated FRET donor in their designed nanoprobe allowed a 10pM limit of detection. Thus, these researchers demonstrated that [R6G][F9-Al] was successfully employed as a visualization agent for potential development of a point of care ratiometric imaging method.

In another study, McNeel et al. expanded upon counterion metathesis by synthesizing a strategic three-component nanoGUMBOS compound for selective imaging of breast cancer cells [27]. Two of three components selected were dianionic fluorescein ($[FL]^{2-}$) and cationic rhodamine B ($[RhB]^{+}$), which could undergo pH-dependent FRET [178]. These researchers approached their triple-GUMBOS synthetic design through pH manipulation with $[FL]^{2-}$, rhodamine B chloride [RhB][Cl], and $[P_{66614}][Cl]$ as a hydrophobic agent, to yield $[P_{66614}][RhB][FL]$ triple GUMBOS. The resultant compound was then employed for nanoGUMBOS synthesis, and when precipitated from water with neutral pH, nanoparticles of approximately 4.4 nm ± 0.7 nm were obtained. However, when using other pH values for nanoGUMBOS synthesis, these researchers determined that nanoGUMBOS sizes and size distributions varied. Absorbance and fluorescence emission properties from low to high pH values were reported, and noticeable ratiometric changes in spectra were observed. A linear ratiometric trend corresponding to pH-dependent FRET responses was observed between moderate pH values (approximately pH 5.0 to 7.0), from which quantitative information may be derived. To further demonstrate the applicability of this three-component nanoGUMBOS system, these investigators also conducted fluorescence microscopy imaging studies with normal and cancerous breast cells. These studies demonstrated that nanoGUMBOS maintained clear selectivity for breast cancer cells since, as cells were illuminated. In contrast, normal cells remained dim. Therefore, three-component nanoGUMBOS were determined useful for both pH sensing and fluorescence imaging of breast cancer cells without the use of polymer encapsulation [27].

Another application for FRET-based sensing of solid-state ionic materials is described by Ashokkumar et al. [179]. In this work, oxygen sensing nanoparticle probes for cellular systems were developed using a polymer encapsulated novel cyanine dye called $[BlueCy]^{+}$ tetrakis(pentafluorophenyl) borate ($[F5\text{-}TPB]^{-}$) or [BlueCy][F5-TPB] that was also loaded with oxygen sensing platinum octaethylporphyrin (PtOEP) as a FRET acceptor. In this case, $[BlueCy]^{+}$ was designed as FRET donor and synthesized from two cyanine dyes: 2-methyl-3-octadecylbenzo[d] thiazol-3-ium iodide and 3-methyl-2-(methylthio)benzo[d]thiazol-3-ium iodide. After dye encapsulation into poly(methyl methacrylate-co-methacrylic acid) and poly(lactic-co-glycolic acid), PMMA-MA and PLGA, respectively, it was determined that both dyes were successfully incorporated into PMMA-MA. Nanoparticle sizes, PtOEP loading, and photophysical properties were evaluated. These investigators determined that dye encapsulated PMMA-MA nanoparticles were 40 nm in diameter with 17% QY after reprecipitation from dioxane. Moreover, after testing several ratios of donor dye loadings, ratios of 1:100 (PtOEP:[BlueCy][F6-TPB]) demonstrated good FRET efficiency. Solution based experiments for oxygen sensing were performed, and ratiometric trends were demonstrated for oxygen rich and poor environments. After confirming low phototoxicity when incubated with HeLa cells, the investigators conducted further studies with FRET nanoparticles in low and normal oxygen environments. HeLa cells were incubated with FRET nanoparticles in a microfluidic device, and an oxygen gradient was introduced by application of an oxygen scavenger. Resultant emission gradients were observed after fluorescent microscopic images were obtained. Ultimately, these researchers

demonstrated the utility of their nanoprobe for detection of cancer cells via microfluidic application. As a result, the authors concluded that this probe could also be used to visualize oxygen gradients in cancerous cells.

In another study from the Warner research group, nanoGUMBOS were synthesized and evaluated as ratiometric sensors for reactive oxygen species (ROS) [42]. Cong et al. designed binary nanoGUMBOS using reprecipitation of 1,1′-diethyl-2,2′-cyanine and 1,1′-diethyl-2,2′-carbocyanine bis(perfluoroethylsulfonyl) imide ([PIC][NTf_2] and [PC][NTf_2], respectively). Optimal FRET efficiency was determined to be 10:1 [PIC]:[PC] molar ratio, and binary nanoparticles shapes were classified as nanodiamonds with spectrally consistent J-aggregation. Analysis of variance (ANOVA) was employed to investigate reactivity of ROS with nanoGUMBOS. Significant differences were observed for hydroxyl radical ($^{\bullet}OH$) over four other evaluated ROS, indicating selectivity of this binary nanoGUMBOS system toward $^{\bullet}OH$ species. Moreover, these investigators observed a linear trend for ratiometric sensing of this probe at various concentrations of $^{\bullet}OH$ in the presence of singlet oxygen ($^1O_2$). Further, potential applications in imaging were investigated, nanoGUMBOS were incubated with breast cancer cells and exposed to oxidative stress. Fluorescence emission changes before and after oxidative stress indicated results in agreement with solution-based studies. Therefore, a binary ratiometric nanoGUMBOS probe was developed for potential quantitative ROS imaging studies using a facile method.

3.2 Differential sensing: biological applications

Biosensing of mixtures of biomarkers and/or proteins is of particular interest for disease diagnosis and treatment [180–182]. Many current methods, such as enzyme-linked immunosorbent assay (ELISA) or polyacrylamide gel electrophoresis (PAGE) coupled to mass spectrometry, require expensive resources and labor intensive steps [182–184]. Organic salts are of increasing interest for development of fluorescent sensor arrays for protein detection and discrimination as they are easily tunable for increasing hydrophobicity, traditionally more stable upon ion exchange, and require little resources for purification [90].

Galpothdeniya and coworkers used partially selective 6-(p-toluidino)-2-naphthalenesulfonate sodium salt ([TNS][Na]) in an ion exchange metathesis reaction with cations tetrabutylphosphonium ($[P_{4444}]^+$), benzyltriphenylphosphonium ($[BTP]^+$), 4-nitrobenzyltriphenylphosphonium ($[4NBP]^+$), and tetraphenylphosphonium ($[TPP]^+$) in order to obtain four different GUMBOS [59]. These investigators rationalized that, as a result of partial selectivity to hydrophobic regions of proteins, TNS-based GUMBOS would make facile, suitable candidates to generate a sensor array for proteins. Proteins such as human serum albumin (HSA), fibrinogen, α-antitrypsin (α-Ant), immunoglobulin G (IgG), β-lactoglobulin (β-Lac), ribonuclease A (RNaseA), α-chymotrypsin (α-CTP), transferrin (Trans), lysozyme (Lys) were used for sensor array development. Sensor responses were collected at various concentrations of proteins.

As a result of notably larger sensor responses, [TNS]-based GUMBOS were determined to have highest sensitivity to HSA, α-Ant, and β-Lac proteins. For this reason, the investigators employed responses for sensor responses to different concentrations of HSA, α-Ant, and β-Lac for multivariate analysis. Both sensor response values and corresponding protein concentrations were employed to build a principal component analysis (PCA) model. By employing the first two principal components (PCs), which accounted for 99.72% of the variance, a linear discriminant analysis (LDA) model with cross-validation was constructed reaching 100% discrimination

accuracy. These researchers noted that the highest sensor responses were obtained for HSA and α-Ant. Thus, these sensor responses were employed to generate anther PCA model in order to evaluate discrimination between these two proteins regardless of protein concentration. In this model, the first two PCs accounted for 99.91% variance, and LDA with cross-validation resulted in 91.7% accuracy. To improve this accuracy, these investigators normalized sensor responses for each protein, constructed a PCA model with the first three PCs corresponding to 98.29% variance. These three PCs were employed for LDA construction and, with cross-validation, accuracy resulted in 100% discrimination. Furthermore, five mixtures of different HSA: α-Ant ratios were evaluated for mixture discrimination analysis. In this case, PCA followed by LDA resulted in 100% discrimination accuracy. Thus, TNS-GUMBOS were evaluated and confirmed as useful materials for protein sensor arrays for analyses of serum proteins HSA, α-Ant, and β-Lac.

More recently, Pérez and coworkers developed a nanoGUMBOS sensor array based on three fluorescent thiacarbocyanine ($[TC0]^+$, $[TC1]^+$, and $[TC2]^+$) dyes with two anions ($[BETI]^-$ and $[NTf_2]^-$) for discrimination of several proteins [182]. NanoGUMBOS and microGUMBOS of these six compounds varied in size and shape, from circular shapes with $[TC0][NTf_2]$ and sizes around 25 nm, to [TC1][BETI] with rod-like shapes and an average size of 1.2 ± 0.5 μm by 0.21 ± 0.08 μm, and $[TC2][NTf_2]$ displayed triangular profiles with average dimensions 200 ± 10 nm by 177 ± 80 nm. Aggregates of nanoGUMBOS of [TC0]- and [TC2]-GUMBOS exhibited absorbance spectral characteristics representative of H-aggregation, while [TC1][NTf2] and [TC1][BETI] both resulted in spectral peaks representative of J-aggregation.

In the above study, seven proteins were investigated, including the four most abundant serum proteins: HSA, IgG, transferrin (Trans), and fibrinogen (Fib), along with three non-serum proteins hemoglobin (Hb), cytochrome C (CytC), and lysozyme (Lys), with each protein exhibiting different physical characteristics. The investigators observed different response patterns for each protein. In this work, these researchers determined that employing raw data was optimal for constructing an LDA model, in which 100% discrimination accuracy of proteins was achieved. Among different protein concentrations, sensor responses were determined to be stable between 0.1 to 20 μg/mL. Mixtures of two proteins, HSA and Hb, were also investigated in this work. Various weight ratios of HAS:Hb mixtures from 100% HSA to 100% Hb, were evaluated and 100% accuracy was achieved when LDA was constructed using these response patterns. However, 80:20 HSA:Hb was observed to be an outlier with the lowest canonical score values, and further analysis using hierarchical cluster analysis determined this dataset to be less related to other ratios. Protein spiked artificial urine with 5 μg/mL protein concentration was employed to evaluate sensor array performance in real samples, and LDA model performance achieved 100% discrimination accuracy. Thus, a series of TC-based GUMBOS were successfully synthesized into nanoGUMBOS and microGUMBOS and developed as protein sensor arrays capable of 100% discrimination in complex mixtures.

3.3 Differential sensing: volatile organic compounds

ILs have been explored for quartz crystal microbalance (QCM) applications as chemosensors for detection and discrimination of volatile organic compounds (VOC) [185–188]. However, for these investigations, differentiation of VOCs sensor response relied on concentration and molecular composition of an analyte. In 2012, Regmi and coworkers developed a system to correlate sensor responses using GUMBOS-polymer composite [75]. In this work, investigators characterized and

explored the responses of cellulose acetate and 1-butyl-2,3-dimethylimidazolium hexafluorophosphate (CA-[BM_2IM][PF_6]). By carefully evaluating characteristic responses upon exposure to control sensors, composite material, and confirming results using molecular dynamic simulations, investigators determined that sensor response recorded as changes in frequency were directly proportional to changes in motional resistance. Thus, these researchers successfully derived molecular weight trends from their composite sensor.

Another exploration demonstrated that counterion exchange using only GUMBOS coatings on quartz crystal resonators (QCRs) could provide VOC differentiation. In 2015, Regmi et al. explored trihexyltetradecylphosphium copper phthalocyanine-3,4′,4″,4‴-tetrasulfonic acid ([P_{66614}]$_4$[$CuPcS_4$]) and trihexyltetradecylphosphium copper(II) meso-tetra(4-carboxyphenyl)porphyrin ([P_{66614}]$_4$[CuTCPP]) as sensing materials [73]. Each GUMBOS sensor successfully allowed detection of a variety of VOCs, such as acetone, acetonitrile, nitromethane, toluene, chloroform ($CHCl_3$), methanol (MeOH), ethanol (EtOH), 2-propanol, 1-propanol, 1-butanol, and 3-methyl-1-butanol. Both sensor responses readily allowed detection of multiple alcohols at relatively low detection limits when compared to other polar and nonpolar analytes. When compared to IL trihexyltetradecylphosphium bis(trifluoromethanesulfonimide), [P_{66614}]$_4$[CuTCPP] provided higher frequency response signals upon exposure to MeOH vapor, and more rapidly achieved baseline with efficient replicate results. Thus, these investigators demonstrated that use of copper(II) porphyrin counterion in GUMBOS allowed investigators to achieve high selectivity in sensor responses to VOCs [73]. Since these reports, there have been other explorations into IL and/or polymer-IL composite responses for VOC detection, and many have attained discrimination via statistical techniques to access virtual and multi-sensor arrays [69–72, 189].

Since VOCs are frequently found as complex mixtures, Vaughan et al. have proposed development of a multi-sensor array (MSA) employing copper(II) phthalocyanine or [$CuPcS_4$]-based GUMBOS sensors [68]. An example of such a sensory coating scheme is shown in **Figure 6**. VOCs studied represent compounds from different classes, such as dichloromethane (DCM), MeOH, 1-propanol, toluene, $CHCl_3$, heptane, hexane, and benzene. In this work, [P_{4444}]$^+$, tributyl-n-octylphosphonium ([P_{4448}]$^+$), tetrabutylammonium ([TBA]$^+$), 3-(dodecyldimethyl-ammonio)propanesulfonate ([DDMA]$^+$) were employed as cations for [$CuPcS_4$]$^{4-}$ to generate four different sensory coatings. Each coating displayed different layering characteristics as determined by SEM. Upon exposure to VOCs, each sensor presented analyte specific response patterns. Using original data, and quadratic discriminant analysis (QDA) with cross-validation, the resultant accuracy was determined to be 98.6%.

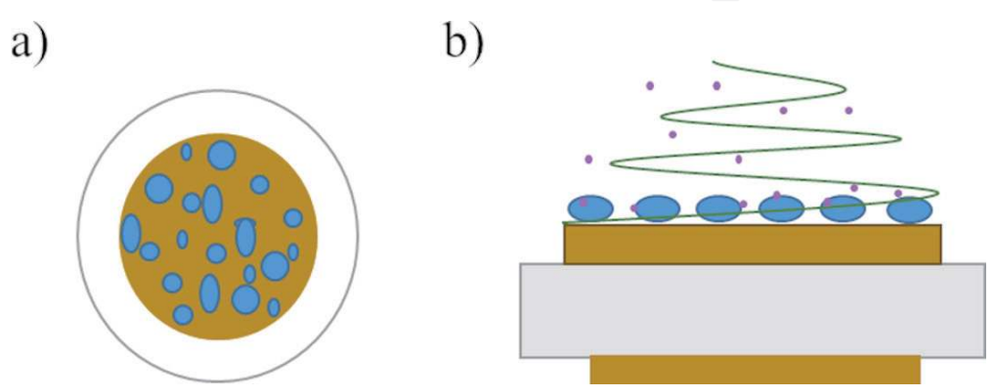

Figure 6.
(a) Representative example of GUMBOS coated QCR; (b) analyte sensing and harmonic wave pattern of QCR on electrode surface.

Thus, $[CuPcS_4]$-based GUMBOS responses were successfully employed to build a VOC-MSA to achieve high accuracy discrimination [68].

4. Optoelectronic developments

With increasing global commercialization of state-of-the-art optoelectronic displays, the demand for higher performance and flexible materials has also increased [107–110]. In general, these devices are comprised of emissive layers between electrodes along with several other electronically active layers. Organic light emitting diodes (OLEDs) and organic photovoltaics (OPVs) have been the central target for a multitude of research groups, from organic emissive layer development to full device performance [107–111]. Counterion strategies using cations and anions within active layers for enhancement on optoelectronic device fabrication to effects on emission and device function will be discussed in the following sections.

4.1 Counterion strategies for light emissive layers in OLEDs

Scientists have optimized several characteristics for targeted OLED development where they require consistent uniformity of emissive layers for potential manufacturing production [190], low crystallinity to prevent non-linear optical activity [191, 192], resistance to oxidation and water [193], and high thermal stability and optical purity [194]. Ionic transition metal complexes (ITMCs) are of huge interest as a wide range of emissive hues is easily achievable, synthesis is relatively simple, and they have desirable luminescent properties [195]. However, traditional methods of OLEDs fabrication involves vacuum evaporation deposition, or vacuum thermal evaporation (VTE) [196], which involves uniform coating of emissive layers [197].

In this regard, Dongxin Ma and coworkers have investigated four cationic iridium complexes as candidates for VTE through counterion control [195]. By incorporating large non-coordinating anions, these investigators achieved VTE iridium-based ionic emissive layers. The anions $[PF_6]^-$, $[TPFB]^-$, and tetrakis[3,5-bis(trifluoromethyl)phenyl]borate ($[BArF]^-$) were employed for quantum chemical calculations, and the investigators determined that distances between iridium and boron atoms were larger than 8 Å with both $[TPFB]^-$ and $[BArF_{24}]^-$ counterions. In comparison, distances between iridium and phosphorous was determined to be 6 Å, as a result of a larger partial positive charge on the phosphorous atom. Compounds synthesized from metathesis with bulkier anions $[TPFB]^-$ and $[BArF_{24}]^-$ were employed for device fabrication using VTE as larger interatomic distances were presumed more suitable for phase transition, and device performance was evaluated. These investigators found devices ranged from blue to red-orange with external quantum efficiencies (EQEs) ranging from 1.2% (blue emission) to 8.1% (yellow emission) [195]. In 2018, these anions were also employed to produce two red-orange devices based on cationic iridium compounds, and these compounds were useful as dopants in 4,4′,4″-tris(carbazol-9-yl)triphenylamine emissive layers (TCTA) to produce white OLEDs with Commission Internationale de L'Eclairage (CIE) coordinate values equal to (0.33, 0.34), that were near to the required values (0.33, 0.33) [198].

More recently, Bai and coworkers investigated counterion-tuning strategies for a sky-blue fluorescent Ir-cation for VTE [199]. Instead of boron-based anions to improve VTE, the investigators strategically focused on bulky sulfonate-containing anions that also contained electron-deficient oxadiazole and triazine structures, such as 3,5-bis(5-(4-(tert-butyl)phenyl)-1,3,4-oxadiazol-2-yl)benzenesulfonate ($[OXD\text{-}7\text{-}SO_3]^-$), 4-(4,6-diphenyl-1,3,5-triazin-2-yl)benzenesulfonate

([TRZ-p-SO_3]$^-$), and 3-(4,6-diphenyl-1,3,5-triazin-2-yl)benzenesulfonate ([TRZ-m-SO_3]$^-$). These structures were expected to not only provide VTE capabilities, but also improve carrier transport and trapping efficiencies that would improve overall efficiency and blue-emission of OLEDs. These researchers concluded that devices fabricated with [TRZ-m-SO_3]$^-$ and [TRZ-p-SO_3]$^-$ anions resulted in better overall device performances, slightly decreased CIE x-coordinate value, and displayed the largest external quantum efficiencies (EQEs) of 12.3 and 12.4%, respectively [199].

Carbazole-containing compounds with expanded conjugation are known to provide efficient blue emission, although they often require high labor and resource costs. In this regard, Siraj et al. synthesized carbazole imidazolium iodide ([CI][I]) along with analogues containing [OTf]$^-$, [NTf_2]$^-$, and [BETI]$^-$ anions as respective GUMBOS in an efficient manner [54]. These GUMBOS were then compared to parent [CI][I] to evaluate counterion effects on thermal and photochemical properties that relate to performance for blue-emitters for OLEDs. In this study, non-uniform packing was observed in all GUMBOS as a result of cation structure. All ion-exchanged GUMBOS also demonstrated significantly higher thermal stabilities with onset degradation temperatures ranging from 310 to 417 °C as determined by thermal gravimetric analysis (TGA), where increasing size of anion yielded increased degradation temperature ([I] < [OTf]$^-$ < [NTf_2]$^-$ < [BETI]$^-$). Similarly, QYs were increased with ion exchanges. In methanolic solution, [CI][BETI] was determined to have the largest QY of 99%, followed by [CI][OTf] with 94%, [CI][NTf_2] with 73%, and [CI][I] with 25%. Thus, this demonstrated that hydrophobic counterion exchange affects photophysical properties of the CI-cation.

While VTE has dominated OLED manufacturing, it often requires expensive equipment and is both energy and time consuming [200]. For this reason, several researchers have explored solution processing methods, such as spin coating [200], electrospray deposition [54], along with other methods [201, 202] to provide faster, more inexpensive fabrication procedures [203]. In this report, [CI][OTf], [CI][NTf2], and [CI][BETI] GUMBOS were used to fabricate thin films on quartz glass with electrospray deposition [204], and uniform coating was achieved and confirmed by scanning electron microscopy and fluorescence microscopic analysis. Solid-state emission spectra displayed very slight red-shifting from methanolic spectra of ion-metathesis GUMBOS. In addition, photostabilities were investigated, and [CI][BETI] displayed an irradiation-induced increase in photostability. In contrast, [CI][OTf] and [CI][NTf_2] were relatively stable while irradiated for 3000 s. Moreover, cyclic voltammetry and quantum chemical calculations further supported spectral properties of evaluated CI-based GUMBOS.

In 2016, Zhang and coworkers designed a novel cyanopyridinium stilbene cation ([Py]$^+$) in order to examine the influence of counterion effects on solid-state photophysical properties [205]. Chloride ([Cl]$^-$), nitrate ([NO_3]$^-$), tosylate ([OTs]$^-$), and [TPB]$^-$ anions were employed in this study to form Ion pairs, and the resultant compounds showed little fluorescence in solution. When explored as films, blue-shifting of emission peaks occurred and increased with increasing hydrophobicity of counterions; QYs also increased following this trend. However, [Py][TPB] GUMBOS were non-emissive in solid-state. In order to understand this variance in trend, investigators used X-ray crystallography and quantum chemical calculations. From these studies, the authors determined that dimeric fluorophore aggregates were responsible for emission in GUMBOS. In [Py][TPB], fluorophores became dilute as a result of bulky anions, resulting in very weak fluorescence emission. This was also confirmed in quantum chemical studies, where intramolecular charge transfer characteristics were confirmed through prediction of frontier molecular orbital placement to reveal donor-σ-acceptor properties for dimeric stacking.

In another study, expansion of applications of the propidium dication ($[P]^{2+}$) was investigated by exchanging iodide counterions for $[OTf]^-$, $[NTf_2]^-$, and $[BETI]^-$ anions to generate P-based GUMBOS for potential solid-state applications [53]. Thermal, spectral, photo-physical, computational, and electrochemical properties were investigated for all P- based GUMBOS. While [P][OTF] retained physical properties similar to parent dye, such as solubility in more polar solvents, thermal degradation, and higher relative crystallinity, similar to the parent compound. In contrast, $[P][NTf_2]$ and [P][BETI] GUMBOS were more soluble in hydrophobic solvents, more amorphous, and displayed higher thermal stability. A trend was observed where increasing solvent hydrophobicity increased fluorescence lifetime and QY values. The highest fluorescence lifetime and QY for [P][BETI], followed by $[P][NTf_2]$, was observed in DCM. In this regard, the authors proposed that this effect may be a result of hydrophobic counterion stabilization of excited-state $[P]^{2+}$, a phenomenon that resembles the original sensing behavior of the parent compound [P][I] [206]. These investigators also performed cyclic voltammetry to determine oxidation and reduction potentials for each P-based GUMBOS, as well as solution-phase QY calculations. It was determined through computational experiments that electronic transitions would lead to an increased propensity for torsional twisting in the solid state [207]. From these studies, the authors concluded that by simple counterion exchange, applications for propidium dication may be expanded beyond biological probes to potential candidates in optoelectronic devices [53].

4.2 Recent advances in dye-sensitized solar cells

Dye-sensitized solar cells (DSSCs) are an emerging next-generation technology in OPVs [208]. Through intrinsic characteristics such as natural transparency, good efficiency in low light conditions, flexible substrate production and more, applications may be expanded to windows, indoor fixtures, and wearable electronics [209, 210]. Incorporation of two or more complementary sensitizing dyes allows for potential absorption of all wavelengths of sunlight to achieve much higher power conversion efficiencies (PCEs) [208, 211–214]. When implemented in this field, tunable investigations of co-sensitizing dyes that are also ionic and primarily limited to structural variations of zwitterionic squaraine-heptamethine structures rather than ion pairs [215, 216]. Polymethine, or cyanine dyes, however, have been extensively studied in OPV technologies, and several groups have begun explorations into counterion application in DSSCs [217–222].

In 2012, Jordan et al. from the Warner research group reported synthesis and characterization of $[PIC][NTf_2]$ and [PIC][BETI], along with fabrication of respective nanoGUMBOS [36]. Optical properties were compared to the parent [PIC][I], and nanoGUMBOS were synthesized and characterized using TEM and scanning electron microscopy (SEM). Optical properties of the resultant PIC-based nanoGUMBOS were also investigated. These investigators concluded that $[PIC][NTf_2]$ nanodiamonds resulted in a significant increase in fluorescence emission intensity, which could be a result of J-aggregation. The authors hypothesized that [PIC][BETI] nanorods from H-aggregates only slightly increased fluorescence intensity. In 2014, Sarkar and coworkers investigated morphology, size, and current–voltage characteristics of these PIC-based nanoGUMBOS using atomic force microscopy (AFM) and conductive probe-AFM (CP-AFM) [56]. Results from CP-AFM indicated that when the voltage was swept between 1 and − 1 Volts, current values within the range of approximately 10^{-7} to 10^{-8} Amps could be achieved. Raman spectroscopy was employed to monitor anion effects on aggregation changes via changes in intensity. These researchers confirmed that $[PIC][NTf_2]$

nanoGUMBOS exhibited J-aggregation while H-aggregation was observed in [PIC][BETI] nanoGUMBOS. Thus, researchers from both investigations showcased anion dependent nanoparticle morphology and respective effects on spectral and electrochemical properties of broadly absorbing PIC-based nanoGUMBOS that had potential uses in DSSCs.

Kolic et al. have investigated different GUMBOS, including the aforementioned PIC-based GUMBOS, to determine effects on DSSC performances [34]. These dyes were employed as energy relay dyes (ERDs) in electrolyte solutions, where FRET occurs to donate electrons from ERD molecules in electrolyte solution to photosensitizing dye at the electrode surface. **Figure 7** represents a proposed scheme for electron transfer processes involving GUMBOS-ERDs DSSCs. Photoactive dyes such as rhodamine B ($[RhB]^+$), $[PIC]^+$, thiacarbocyanine ($[TC1]^+$), and tetracarboxyphenylporphine ($[TCPP]^{4-}$) precursors underwent ion exchange with appropriate counterions, such as $[NTf_2]^-$, $[BETI]^-$, and $[P_{66614}]^+$, and were further evaluated for counterion effects on ERD performance. Among various GUMBOS studies, investigators determined that $[RhB][NTf_2]$ and $[P_{66614}]_4[TCPP]$ GUMBOS yielded most promising PCEs devices. These investigators hypothesized that this was a result of inherent high molar extinction coefficients and QYs for these respective compounds. They also noted that devices employing $[NTf_2]^-$ anions resulted in higher respective device efficiencies than those of the parent dye or $[BETI]^-$ anions. One deviation of this trend, however, was the case of [TC1][TPB], which demonstrated a much higher QY. Overall, these authors were able to elucidate anion trends for GUMBOS-ERDs and confirm their utility as FRET cosensitizing agents in DSSCs [34].

Other works have recently focused on incorporating metal-based GUMBOS as redox shuttles for sensitizer regenerating agents in DSSCs as well. In 2016, Huckaba and coworkers employed a cobalt(II/III) redox shuttle ($[Co(bpy)_3]^{2+/3+}$) with $[NTf_2]^-$ as a non-coordinating anion with indolizine sensitizers [223]. Device PCEs ranged from 3.04 to 8.10% efficiencies, which were comparable to employing common redox shuttle, iodide/triiodide (I^-/I_3^-) (3.74–7.99%). Additionally, a copper(I/II) redox shuttle ($[Cu(tmby)_2]^{+/2+}$) with $[NTf_2]^-$ counterion was recently employed with indoline derivatives as sensitizers [224]. This study determined that this redox system rapidly regenerated indoline dyes within the range of tens of nanoseconds, several orders of magnitude faster than cobalt(II/III) shuttle $[Co(bpy)_3]^{2+/3+}[NTf_2]_{3/2}$ [224]. As a result of the volatility of the organic solvent employed in electrolyte solutions, some groups have expanded investigations into non-volatile routes for DSSC fabrication [211, 225, 226]. Cao and coworkers have developed a solid-state DSSC (ssDSSC) based on $[Cu(tmby)_2]^{+/2+}[NTf_2]_2$ redox shuttle for a hole transport layer [227]. In comparison to other copper redox shuttles, PCEs were

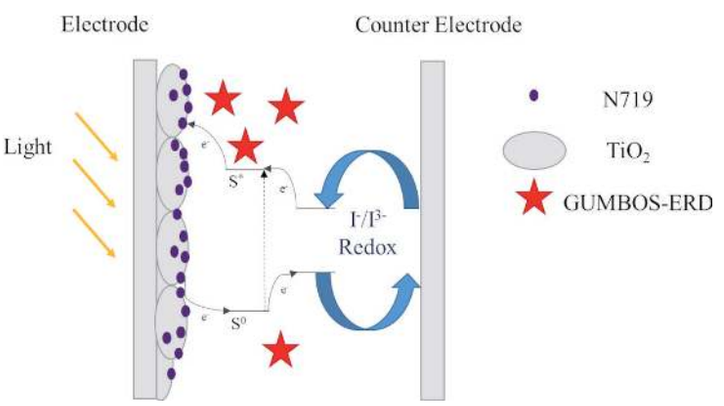

Figure 7.
Schematic of DSSCs fabricated with GUMBOS-ERDs and potential operational mechanism [34, 208].

determined to be much higher with this novel ssDSSC at 11% versus 4.5 or 2%, respectively. Thus, using their trilayered approach with co-sensitizer (Y123) and their solid-state hole transport material, scientists successfully demonstrated charge separation in a novel ssDSSC.

4.3 Organic salts to reduce work function in optoelectronics

Work function (WF) is a metric by which charge transfer at electrodes is measured to determine electron injection efficiencies of optoelectronics [228]. For this reason, many groups have targeted improving device efficiency by optimizing charge transport at interfacial layers by including electroactive coatings[228–230]. Incorporating ethoxylated polyethylenimine (PEIE) at electrode interfaces of OLEDs was previously demonstrated by Zhou and coworkers to reduce WF [231]. In 2019, Ohisa et al. hypothesized that incorporation of tetraalkylammonium salts ([TRA][X]) into PEIE layers could further reduce required WFs for OLEDs [231, 232]. Alkyl chain lengths that varied between tetraethyl ($[TEA]^+$), tetrabutyl ($[TBA]^+$), and tetrahexyl ($[THA]^+$) ammonium groups were studied in this report. Different anions were employed, and a series of salts were investigated for each ammonium cations. Anions employed ranged from $[Cl]^-$, bromine ($[Br]^-$), $[I]^-$, acetyl ($[Ac]^-$), thiocyanate ($[SCN]^-$), or tetrafluoroborate ($[BF_4]^-$). Ultimately, 30 wt % [TBA][X] incorporation into PEIE layer at cathode interfaces improved WF as determined by ultraviolet photoelectron spectroscopy [232]. Researchers determined that anions with strong electron donating characteristics, such as $[SCN]^-$ and $[Ac]^-$, resulted in the largest reduction of WF, while small halides provided the lowest WF change.

Investigators continued their investigations with chain length studies using [TEA][Cl] and [THA][Cl] dopants in PEIE electrode coatings and studying WF values. Results indicated that longer chain lengths provided larger steric hindrance, and thus, weaker electron accepting ability. Overall, WF decreased as hypothesized; however, devices with PEIE:[TBA][SCN] doping resulted in an unexplained increase in drive voltage. In general, this work demonstrates anion influence on WF and electronic efficiencies in LEDs [232]. More recently, Duan and coworkers expanded this work to include anion exchange effects on polyelectrolytes inspired by PEIE design [233]. These investigators incorporated ammonium cations into the PEIE backbone and used several sulfonate anions, such as dimethyl sulfonate ($[MSB]^-$), benzylsulfonate ($[BSB]^-$), and diethyl sulfonate ($[ESB]^-$), to examine effects on WF for polymer solar cells. Notably, these researchers found that smaller anions, e.g. $[ESB]^-$ and $[MSB]^-$, yielded devices with more efficient electron transport characteristics and better performance than devices with $[BSB]^-$. Interestingly, devices with [PEIE][ESB] demonstrated the highest PCE (10.44%) with 8 nm thickness at minimal light soaking [233].

In another work, Sato and coworkers investigated counterion exchange effects on a polymerized IL system to reduce WF at the electron-injection layer to provide sufficient electrons to the semiconducting layer [231]. These investigators employed two fluorinated anions to produce polydiallylammonium polymeric ILs [poly(DDA)][NTf_2] and [poly(DDA)][BETI], respectively. Both polymers were evaluated and compared to their parent PIL [poly(DDA)][Cl]. Hydrophobicities were studied via water contact angle measurements between film samples and water droplets. As anticipated, larger contact angles were observed for the more hydrophobic anions $[NTf_2]^-$ and $[BETI]^-$ as compared with $[Cl]^-$, 80.1, 80.8 and 19.1°, respectively. Noticeable increases in 5% onset degradation temperatures of the polymers were also observed upon conversion from PIL to polymer-ion exchanges, from 285 °C in [poly(DDA)][Cl] to 394 and 395 °C with [poly(DDA)][NTf_2] and [poly(DDA)][BETI], respectively. Both ion-exchanged polymer-ILs reduced WF when they

were incorporated at the cathode interface and increased WF when employed at the anode, which indicates that they are suitable interfacial coatings for OLED development. After device optimization as electron injection layers, the authors reported a best device performance of 9.00% maximum EQE with [poly(DDA)][NTf_2]. Overall, these researchers demonstrated the benefits of hydrophobic counterion exchange for PILs and their utility for OLEDs applications at electrode interfaces.

5. Conclusions and future directions

Much like room temperature ILs, the ionic properties of frozen ILs and GUMBOS lend to high tunability as a result of the exponential combinations possible of known anions and cations. This important characteristic allows for strategic design of specific GUMBOS for a targeted analytical task. This chapter summarized a few examples of possible GUMBOS applications. Moreover, it has been demonstrated that several physico-chemical properties of these compounds are improved in solid state as compared to liquid phase organic salts. For these reasons, we hypothesize that implementation of solid-phase ILs and GUMBOS in the analytical and materials fields will increase in the future.

Acknowledgements

The authors gratefully acknowledge financial support through NASA cooperative agreement NNX 16AQ93A under contract number NASA/LEQSF (2016-2019)-Phase 3-10, and the National Science Foundation under Grant Nos. CHE-1905105 and HRD-1736136. Any opinions, findings, and conclusions or recommendations expressed in this material are those of the author(s) and do not necessarily reflect the views of the National Science Foundation.

Conflict of interest

The authors declare no conflict of interest.

Author details

Rocío L. Pérez, Caitlan E. Ayala and Isiah M. Warner*
Department of Chemistry, Louisiana State University, Baton Rouge, LA, United States

*Address all correspondence to: iwarner@lsu.edu

References

[1] Brown, R.J. and M.J. Milton, *Analytical techniques for trace element analysis: an overview.* TrAC Trends in Analytical Chemistry, 2005. **24**(3): p. 266-274.

[2] Lin, D.C., E.K. Dimitriadis, and F. Horkay, *Robust strategies for automated AFM force curve analysis—I. Non-adhesive indentation of soft, inhomogeneous materials.* 2007.

[3] Dogan-Topal, B., S.A. Ozkan, and B. Uslu, *The analytical applications of square wave voltammetry on pharmaceutical analysis.* The Open Chemical and Biomedical Methods Journal, 2010. **3**(1).

[4] Chakraborty, P. and T. Pradeep, *The emerging interface of mass spectrometry with materials.* NPG Asia Materials, 2019. **11**(1): p. 1-22.

[5] Ambrose, W., et al., *A.; Werner, JH; Keller, RA.* Chem. ReV, 1999. **99**(10): p. 2929-2956.

[6] Pfannmoller, M., et al., *Visualizing a homogeneous blend in bulk heterojunction polymer solar cells by analytical electron microscopy.* Nano letters, 2011. **11**(8): p. 3099-3107.

[7] Commerce, N.I.o.S.a.T.-U.S.D.o., *Available online: Measurements, Standards, and Reference Materials for Industrial Commodities*. 2008.

[8] Ye, F., et al., *A compact and highly fluorescent orange-emitting polymer dot for specific subcellular imaging.* Chemical Communications, 2012. **48**(12): p. 1778-1780.

[9] Ramos, J., et al., *Soft nanoparticles (thermo-responsive nanogels and bicelles) with biotechnological applications: from synthesis to simulation through colloidal characterization.* Soft Matter, 2011. **7**(11): p. 5067-5082.

[10] Tessler, L.A., et al., *Nanogel surface coatings for improved single-molecule imaging substrates.* Journal of the Royal Society Interface, 2011. **8**(63): p. 1400-1408.

[11] Nishiyabu, R., et al., *Confining Molecules within Aqueous Coordination Nanoparticles by Adaptive Molecular Self-Assembly.* Angewandte Chemie, 2009. **121**(50): p. 9629-9632.

[12] Ojida, A., et al., *Turn-on fluorescence sensing of nucleoside polyphosphates using a xanthene-based Zn (II) complex chemosensor.* Journal of the American Chemical Society, 2008. **130**(36): p. 12095-12101.

[13] Cole, M.R.H., J.A.; Warner, I.M., *Recycling Antibiotics into GUMBOS: A New Combination Strategy to Combat Multi-Drug-Resistant Bacteria.* Molecules. **20**: p. 6466-6487.

[14] Cole, M.R., et al., *Minimizing human infection from Escherichia coli O157:H7 using GUMBOS.* Journal of Antimicrobial Chemotherapy, 2013. **68**(6): p. 1312-1318.

[15] Cole, M.R., et al., *Design, Synthesis, and Biological Evaluation of β-Lactam Antibiotic-Based Imidazolium- and Pyridinium-Type Ionic Liquids.* Chemical Biology & Drug Design, 2011. **78**(1): p. 33-41.

[16] Chen, M., et al., *Mitochondria targeting IR780-based nanoGUMBOS for enhanced selective toxicity towards cancer cells.* RSC Advances, 2018. **8**(55): p. 31700-31709.

[17] Bhattarai, N., et al., *Enhanced chemotherapeutic toxicity of cyclodextrin templated size-tunable rhodamine 6G nanoGUMBOS.* Journal of Materials Chemistry B, 2018. **6**(34): p. 5451-5459.

[18] Bhattarai, N., et al., *Endocytic Selective Toxicity of Rhodamine 6G*

nanoGUMBOS in Breast Cancer Cells. Molecular Pharmaceutics, 2018. **15**(9): p. 3837-3845.

[19] Das, S., et al., *Multimodal theranostic nanomaterials derived from phthalocyanine-based organic salt.* RSC Advances, 2015. **5**(38): p. 30227-30233.

[20] Siraj, N., et al., *Strategy for Tuning the Photophysical Properties of Photosensitizers for Use in Photodynamic Therapy.* Chemistry – A European Journal, 2015. **21**(41): p. 14440-14446.

[21] Dumke, J.C., et al., *In vitro activity studies of hyperthermal near-infrared nanoGUMBOS in MDA-MB-231 breast cancer cells.* Photochemical & Photobiological Sciences, 2014. **13**(9): p. 1270-1280.

[22] Magut, P.K.S., et al., *Tunable Cytotoxicity of Rhodamine 6G via Anion Variations.* Journal of the American Chemical Society, 2013. **135**(42): p. 15873-15879.

[23] Dumke, J.C., et al., *Photothermal Response of Near-Infrared-Absorbing NanoGUMBOS.* Applied Spectroscopy, 2014. **68**(3): p. 340-352.

[24] Li, M., et al., *Lipophilic phosphonium–lanthanide compounds with magnetic, luminescent, and tumor targeting properties.* Journal of Inorganic Biochemistry, 2012. **107**(1): p. 40-46.

[25] McNeel, K.E., et al., *Sodium Deoxycholate Hydrogels: Effects of Modifications on Gelation, Drug Release, and Nanotemplating.* The Journal of Physical Chemistry B, 2015. **119**(27): p. 8651-8659.

[26] McNeel, K.E., et al., *Sodium deoxycholate/TRIS-based hydrogels for multipurpose solute delivery vehicles: Ambient release, drug release, and enantiopreferential release.* Talanta, 2018. **177**: p. 66-73.

[27] McNeel, K.E., et al., *Fluorescence-Based Ratiometric Nanosensor for Selective Imaging of Cancer Cells.* ACS Omega, 2019. **4**(1): p. 1592-1600.

[28] Bwambok, D.K., et al., *Near-Infrared Fluorescent NanoGUMBOS for Biomedical Imaging.* ACS Nano, 2009. **3**(12): p. 3854-3860.

[29] De Rooy, S.L., et al., *Ephedrinium-based protic chiral ionic liquids for enantiomeric recognition.* Chirality, 2011. **23**(1): p. 54-62.

[30] Bwambok, D.K., et al., *Amino Acid-Based Fluorescent Chiral Ionic Liquid for Enantiomeric Recognition.* Analytical Chemistry, 2010. **82**(12): p. 5028-5037.

[31] Li, M., et al., *Combinatorial Approach to Enantiomeric Discrimination: Synthesis and 19F NMR Screening of a Chiral Ionic Liquid-Modified Silane Library.* Journal of Combinatorial Chemistry, 2009. **11**(6): p. 1105-1114.

[32] Li, M., et al., *Magnetic chiral ionic liquids derived from amino acids.* Chemical Communications, 2009(45): p. 6922-6924.

[33] Bwambok, D.K., et al., *Synthesis and characterization of novel chiral ionic liquids and investigation of their enantiomeric recognition properties.* Chirality, 2008. **20**(2): p. 151-158.

[34] Kolic, P.E., et al., *Improving energy relay dyes for dye-sensitized solar cells by use of a group of uniform materials based on organic salts (GUMBOS).* RSC Advances, 2016. **6**(97): p. 95273-95282.

[35] Kolic, P.E., et al., *Synthesis and Characterization of Porphyrin-Based GUMBOS and NanoGUMBOS as Improved Photosensitizers.* The Journal of Physical Chemistry C, 2016. **120**(9): p. 5155-5163.

[36] Jordan, A.N., et al., *Anion-controlled morphologies and spectral features of cyanine-based nanoGUMBOS – an improved photosensitizer.* Nanoscale, 2012. **4**(16): p. 5031-5038.

[37] Berton, P., et al., *Ionic liquid-based dispersive microextraction of nitrotoluenes in water samples.* Microchimica Acta, 2014. **181**(11): p. 1191-1198.

[38] Huang, F., et al., *Surfactant-based ionic liquids for extraction of phenolic compounds combined with rapid quantification using capillary electrophoresis.* ELECTROPHORESIS, 2014. **35**(17): p. 2463-2469.

[39] Deng, N., et al., *Highly efficient extraction of phenolic compounds by use of magnetic room temperature ionic liquids for environmental remediation.* Journal of Hazardous Materials, 2011. **192**(3): p. 1350-1357.

[40] Vidanapathirana, P., et al., *Cationic ionic liquid surfactant-polyacrylamide gel electrophoresis for enhanced separation of acidic and basic proteins with single-step ribonuclease b glycoforms separation.* Journal of Chromatography A, 2017. **1515**: p. 245-251.

[41] Hasan, F., et al., *Ionic liquids as buffer additives in ionic liquid-polyacrylamide gel electrophoresis separation of mixtures of low and high molecular weight proteins.* RSC Advances, 2015. **5**(85): p. 69229-69237.

[42] Cong, M., et al., *Ratiometric fluorescence detection of hydroxyl radical using cyanine-based binary nanoGUMBOS.* Sensors and Actuators B: Chemical, 2018. **257**: p. 993-1000.

[43] Lu, C., et al., *Spectral and Physicochemical Characterization of Dysprosium-Based Multifunctional Ionic Liquid Crystals.* The Journal of Physical Chemistry A, 2015. **119**(20): p. 4780-4786.

[44] Al Ghafly, H., et al., *GUMBOS matrices of variable hydrophobicity for matrix-assisted laser desorption/ionization mass spectrometry.* Rapid Communications in Mass Spectrometry, 2014. **28**(21): p. 2307-2314.

[45] Hamdan, S., et al., *Strategies for controlled synthesis of nanoparticles derived from a group of uniform materials based on organic salts.* Journal of Colloid and Interface Science, 2015. **446**: p. 163-169.

[46] Wright, A.R., et al., *Soft- and hard-templated organic salt nanoparticles with the Midas touch: gold-shelled nanoGUMBOS.* Journal of Materials Chemistry C, 2014. **2**(42): p. 8996-9003.

[47] de Rooy, S.L., et al., *Ionically Self-Assembled, Multi-Luminophore One-Dimensional Micro- and Nanoscale Aggregates of Thiacarbocyanine GUMBOS.* The Journal of Physical Chemistry C, 2012. **116**(14): p. 8251-8260.

[48] Das, S., et al., *Tunable Size and Spectral Properties of Fluorescent NanoGUMBOS in Modified Sodium Deoxycholate Hydrogels.* Langmuir, 2012. **28**(1): p. 757-765.

[49] de Rooy, S.L., et al., *Fluorescent one-dimensional nanostructures from a group of uniform materials based on organic salts.* Chemical Communications, 2011. **47**(31): p. 8916-8918.

[50] Das, S., et al., *Nontemplated Approach to Tuning the Spectral Properties of Cyanine-Based Fluorescent NanoGUMBOS.* Langmuir, 2010. **26**(15): p. 12867-12876.

[51] Tesfai, A., et al., *Controllable Formation of Ionic Liquid Micro- and Nanoparticles via a Melt–Emulsion–Quench Approach.* Nano Letters, 2008. **8**(3): p. 897-901.

[52] Tesfai, A., et al., *Magnetic and Nonmagnetic Nanoparticles from a Group of Uniform Materials Based on Organic Salts.* ACS Nano, 2009. **3**(10): p. 3244-3250.

[53] De Silva, T.P.D., et al., *Influence of Anion Variations on Morphological, Spectral, and Physical Properties of the Propidium Luminophore.* The Journal of Physical Chemistry A, 2019. **123**(1): p. 111-119.

[54] Siraj, N., et al., *Carbazole-Derived Group of Uniform Materials Based on Organic Salts: Solid State Fluorescent Analogues of Ionic Liquids for Potential Applications in Organic-Based Blue Light-Emitting Diodes.* The Journal of Physical Chemistry C, 2014. **118**(5): p. 2312-2320.

[55] Siraj, N., et al., *Enhanced S2 emission in carbazole-based ionic liquids.* RSC Advances, 2015. **5**(13): p. 9939-9945.

[56] Sarkar, A., et al., *Electro-optical characterization of cyanine-based GUMBOS and nanoGUMBOS.* Electronic Materials Letters, 2014. **10**(5): p. 879-885.

[57] Galpothdeniya, W.I.S., et al., *Fluorescein-based ionic liquid sensor for label-free detection of serum albumins.* RSC Advances, 2014. **4**(34): p. 17533-17540.

[58] Galpothdeniya, W.I.S., et al., *Ionic liquid-based optoelectronic sensor arrays for chemical detection.* RSC Advances, 2014. **4**(14): p. 7225-7234.

[59] Galpothdeniya, W.I.S., et al., *Tunable GUMBOS-based sensor array for label-free detection and discrimination of proteins.* Journal of Materials Chemistry B, 2016. **4**(8): p. 1414-1422.

[60] Das, S., et al., *Ionic liquid-based fluorescein colorimetric pH nanosensors.* RSC Advances, 2013. **3**(43): p. 21054-21061.

[61] Galpothdeniya, W.I.S., et al., *Virtual Colorimetric Sensor Array: Single Ionic Liquid for Solvent Discrimination.* Analytical Chemistry, 2015. **87**(8): p. 4464-4471.

[62] Stavrou, I.J., et al., *Facile preparation of polysaccharide-coated capillaries using a room temperature ionic liquid for chiral separations.* ELECTROPHORESIS, 2013. **34**(9-10): p. 1334-1338.

[63] Hamdan, S., et al., *Ionic liquid crosslinkers for chiral imprinted nanoGUMBOS.* Journal of Colloid and Interface Science, 2016. **463**: p. 29-36.

[64] Karam, T.E., et al., *Anomalous Size-Dependent Excited-State Relaxation Dynamics of NanoGUMBOS.* The Journal of Physical Chemistry C, 2015. **119**(50): p. 28206-28213.

[65] Karam, T.E., et al., *Ultrafast and nonlinear spectroscopy of brilliant green-based nanoGUMBOS with enhanced near-infrared emission.* The Journal of Chemical Physics, 2017. **147**(14): p. 144701.

[66] Jordan, A.N., et al., *Tunable near-infrared emission of binary nano- and mesoscale GUMBOS.* RSC Advances, 2014. **4**(54): p. 28471-28480.

[67] Lu, C., et al., *Irradiation Induced Fluorescence Enhancement in PEGylated Cyanine-Based NIR Nano- and Mesoscale GUMBOS.* Langmuir, 2012. **28**(40): p. 14415-14423.

[68] Vaughan, S.R., et al., *Class specific discrimination of volatile organic compounds using a quartz crystal microbalance based multisensor array.* Talanta, 2018. **188**: p. 423-428.

[69] Speller, N.C., et al., *QCM virtual sensor array: Vapor identification and molecular weight approximation.* Sensors and Actuators B: Chemical, 2017. **246**: p. 952-960.

[70] Speller, N.C., et al., *QCM virtual multisensor array for fuel discrimination and detection of gasoline adulteration.* Fuel, 2017. **199**: p. 38-46.

[71] Speller, N.C., et al., *Assessment of QCM array schemes for mixture identification: citrus scented odors.* RSC Advances, 2016. **6**(98): p. 95378-95386.

[72] Speller, N.C., et al., *Rational Design of QCM-D Virtual Sensor Arrays Based on Film Thickness, Viscoelasticity, and Harmonics for Vapor Discrimination.* Analytical Chemistry, 2015. **87**(10): p. 5156-5166.

[73] Regmi, B.P., et al., *Phthalocyanine- and porphyrin-based GUMBOS for rapid and sensitive detection of organic vapors.* Sensors and Actuators B: Chemical, 2015. **209**: p. 172-179.

[74] Regmi, B.P., et al., *Molecular weight sensing properties of ionic liquid-polymer composite films: theory and experiment.* Journal of Materials Chemistry C, 2014. **2**(24): p. 4867-4878.

[75] Regmi, B.P., et al., *A novel composite film for detection and molecular weight determination of organic vapors.* Journal of Materials Chemistry, 2012. **22**(27): p. 13732-13741.

[76] Siraj, N.W., Isiah M. , *Compositions including a ruthenium molecular dye-based GUMBOS, methods of making compositions, methods of use of compositions, and devices using the compositions*. 2015.

[77] Siraj, N.W., Isiah M., *Carbazole based GUMBOS for potential applications as highly efficient Blue OLED's*.

[78] Warner, I.M., Regmi, Bishnu P., El-Zahab, Bilal, Hayes, Daniel J. , *Detection and Molecular Weight Estimation of Organic Vapors Using a QCM Sensor*. 2012.

[79] Trujillo-Rodríguez, M.J., et al., *Advances of Ionic Liquids in Analytical Chemistry.* Analytical Chemistry, 2019. **91**(1): p. 505-531.

[80] Liu, Q., S.Z. El Abedin, and F. Endres, *Electroplating of mild steel by aluminium in a first generation ionic liquid: A green alternative to commercial Al-plating in organic solvents.* Surface and Coatings Technology, 2006. **201**(3-4): p. 1352-1356.

[81] Bai, L., et al., *Effects of nucleators on the thermodynamic properties of seasonal energy storage materials based on ionic liquids.* Energy & Fuels, 2011. **25**(4): p. 1811-1816.

[82] Vekariya, R.L., *A review of ionic liquids: Applications towards catalytic organic transformations.* Journal of Molecular Liquids, 2017. **227**: p. 44-60.

[83] Qiao, Y., et al., *Temperature-responsive ionic liquids: fundamental behaviors and catalytic applications.* Chemical reviews, 2017. **117**(10): p. 6881-6928.

[84] Stracke, M.P., et al., *Hydrogen-storage materials based on imidazolium ionic liquids.* Energy & fuels, 2007. **21**(3): p. 1695-1698.

[85] Mahrova, M., et al., *Pyridinium based dicationic ionic liquids as base lubricants or lubricant additives.* Tribology International, 2015. **82**: p. 245-254.

[86] Zhou, Y. and J. Qu, *Ionic liquids as lubricant additives: a review.* ACS applied materials & interfaces, 2017. **9**(4): p. 3209-3222.

[87] Egorova, K.S., E.G. Gordeev, and V.P. Ananikov, *Biological activity of ionic liquids and their application in pharmaceutics and medicine.* Chemical Reviews, 2017. **117**(10): p. 7132-7189.

[88] Gomes, J.M., S.S. Silva, and R.L. Reis, *Biocompatible ionic liquids: fundamental behaviours and applications.*

Chemical Society Reviews, 2019. **48**(15): p. 4317-4335.

[89] Chen, M., et al., *Tumor-Targeting NIRF NanoGUMBOS with Cyclodextrin-Enhanced Chemo/Photothermal Antitumor Activities.* ACS applied materials & interfaces, 2019. **11**(31): p. 27548-27557.

[90] Warner, I.M., B. El-Zahab, and N. Siraj, *Perspectives on Moving Ionic Liquid Chemistry into the Solid Phase.* Analytical Chemistry, 2014. **86**(15): p. 7184-7191.

[91] MacFarlane, D.R., et al., *Ionic liquids and their solid-state analogues as materials for energy generation and storage.* Nature Reviews Materials, 2016. **1**(2): p. 1-15.

[92] Siegel, R.L., K.D. Miller, and A. Jemal, *Cancer statistics, 2020.* CA: A Cancer Journal for Clinicians, 2020. **70**(1): p. 7-30.

[93] Miller, K.D., et al., *Cancer treatment and survivorship statistics, 2019.* CA: a cancer journal for clinicians, 2019. **69**(5): p. 363-385.

[94] Pearce, A., et al., *Incidence and severity of self-reported chemotherapy side effects in routine care: A prospective cohort study.* PloS one, 2017. **12**(10): p. e0184360.

[95] Nurgali, K., R.T. Jagoe, and R. Abalo, *Adverse effects of cancer chemotherapy: Anything new to improve tolerance and reduce sequelae?* Frontiers in pharmacology, 2018. **9**: p. 245.

[96] Oun, R., Y.E. Moussa, and N.J. Wheate, *The side effects of platinum-based chemotherapy drugs: a review for chemists.* Dalton Transactions, 2018. **47**(19): p. 6645-6653.

[97] Zhang, J., et al., *An updated overview on the development of new photosensitizers for anticancer photodynamic therapy.* Acta Pharmaceutica Sinica B, 2018. **8**(2): p. 137-146.

[98] Sharma, R.A., et al., *Clinical development of new drug–radiotherapy combinations.* Nature reviews Clinical oncology, 2016. **13**(10): p. 627-642.

[99] Pérez-Herrero, E. and A. Fernández-Medarde, *Advanced targeted therapies in cancer: Drug nanocarriers, the future of chemotherapy.* European Journal of Pharmaceutics and Biopharmaceutics, 2015. **93**: p. 52-79.

[100] Li, W., et al., *Mild photothermal therapy/photodynamic therapy/ chemotherapy of breast cancer by Lyp-1 modified Docetaxel/IR820 Co-loaded micelles.* Biomaterials, 2016. **106**: p. 119-133.

[101] Kim, H.S. and D.Y. Lee, *Near-infrared-responsive cancer photothermal and photodynamic therapy using gold nanoparticles.* Polymers, 2018. **10**(9): p. 961.

[102] Paris, J.L., et al., *Nanoparticles for multimodal antivascular therapeutics: Dual drug release, photothermal and photodynamic therapy.* Acta Biomaterialia, 2020. **101**: p. 459-468.

[103] Xu, F., et al., *Loading of indocyanine green within polydopamine-coated laponite nanodisks for targeted cancer photothermal and photodynamic therapy.* Nanomaterials, 2018. **8**(5): p. 347.

[104] Pedersen, P.L., *Tumor mitochondria and the bioenergetics of cancer cells*, in *Membrane anomalies of tumor cells*. 1978, Karger Publishers. p. 190-274.

[105] Carracedo, A., L.C. Cantley, and P.P. Pandolfi, *Cancer metabolism: fatty acid oxidation in the limelight.* Nature reviews Cancer, 2013. **13**(4): p. 227-232.

[106] Liberti, M.V. and J.W. Locasale, *The Warburg Effect: How Does it Benefit Cancer Cells?* Trends in Biochemical Sciences, 2016. **41**(3): p. 211-218.

[107] Nödling, A.R., et al., *Cyanine dye mediated mitochondrial targeting enhances the anti-cancer activity of small-molecule cargoes.* Chemical Communications, 2020. **56**(34): p. 4672-4675.

[108] Bhattarai, N., et al., *Endocytic selective toxicity of rhodamine 6G nanoGUMBOS in breast cancer cells.* Molecular pharmaceutics, 2018. **15**(9): p. 3837-3845.

[109] Gear, A.R., *Rhodamine 6G a potent inhibitor of mitochondrial oxidative phosphorylation.* Journal of Biological Chemistry, 1974. **249**(11): p. 3628-3637.

[110] Modica-Napolitano, J.S., et al., *Rhodamine 123 inhibits bioenergetic function in isolated rat liver mitochondria.* Biochemical and biophysical research communications, 1984. **118**(3): p. 717-723.

[111] Davis, S., et al., *Mitochondrial and plasma membrane potentials cause unusual accumulation and retention of rhodamine 123 by human breast adenocarcinoma-derived MCF-7 cells.* Journal of Biological Chemistry, 1985. **260**(25): p. 13844-13850.

[112] Modica-Napolitano, J.S. and J.R. Aprille, *Basis for the selective cytotoxicity of rhodamine 123.* Cancer research, 1987. **47**(16): p. 4361-4365.

[113] Scaduto Jr, R.C. and L.W. Grotyohann, *Measurement of mitochondrial membrane potential using fluorescent rhodamine derivatives.* Biophysical journal, 1999. **76**(1): p. 469-477.

[114] Ma, X., et al., *A Mitochondria-Targeting Gold–Peptide Nanoassembly for Enhanced Cancer-Cell Killing.* Advanced healthcare materials, 2013. **2**(12): p. 1638-1643.

[115] Hu, Y.-P., et al., *ρ0 tumor cells: a model for studying whether mitochondria are targets for rhodamine 123, doxorubicin, and other drugs.* Biochemical Pharmacology, 2000. **60**(12): p. 1897-1905.

[116] Alford, R., et al., *Toxicity of organic fluorophores used in molecular imaging: literature review.* Molecular imaging, 2009. **8**(6): p. 7290.2009. 00031.

[117] Mosquera, J.s., I. García, and L.M. Liz-Marzán, *Cellular uptake of nanoparticles versus small molecules: a matter of size.* Accounts of chemical research, 2018. **51**(9): p. 2305-2313.

[118] Ernsting, M.J., et al., *Factors controlling the pharmacokinetics, biodistribution and intratumoral penetration of nanoparticles.* Journal of Controlled Release, 2013. **172**(3): p. 782-794.

[119] Duan, X. and Y. Li, *Physicochemical characteristics of nanoparticles affect circulation, biodistribution, cellular internalization, and trafficking.* Small, 2013. **9**(9-10): p. 1521-1532.

[120] Stylianopoulos, T., *EPR-effect: utilizing size-dependent nanoparticle delivery to solid tumors.* Therapeutic delivery, 2013. **4**(4): p. 421-423.

[121] Loftsson, T., et al., *Cyclodextrins in drug delivery.* Expert opinion on drug delivery, 2005. **2**(2): p. 335-351.

[122] Miranda, J.C.d., et al., *Cyclodextrins and ternary complexes: technology to improve solubility of poorly soluble drugs.* Brazilian journal of pharmaceutical sciences, 2011. **47**(4): p. 665-681.

[123] Kuang, Y., et al., *Hydrophobic IR-780 dye encapsulated in cRGD-conjugated solid lipid nanoparticles for NIR imaging-guided photothermal therapy.* ACS Applied Materials & Interfaces, 2017. **9**(14): p. 12217-12226.

[124] Chen, Y., et al., *IR-780 loaded phospholipid mimicking homopolymeric*

micelles for near-IR imaging and photothermal therapy of pancreatic cancer. ACS applied materials & interfaces, 2016. **8**(11): p. 6852-6858.

[125] Xia, F., et al., *Matrix metallopeptidase 2 targeted delivery of gold nanostars decorated with IR-780 iodide for dual-modal imaging and enhanced photothermal/photodynamic therapy.* Acta biomaterialia, 2019. **89**: p. 289-299.

[126] Zhang, C., et al., *A near-infrared fluorescent heptamethine indocyanine dye with preferential tumor accumulation for in vivo imaging.* Biomaterials, 2010. **31**(25): p. 6612-6617.

[127] Choi, J., et al., *Targeting tumors with cyclic RGD-conjugated lipid nanoparticles loaded with an IR780 NIR dye: In vitro and in vivo evaluation.* International Journal of Pharmaceutics, 2017. **532**(2): p. 677-685.

[128] Dai, Q., C. Walkey, and W.C. Chan, *Polyethylene glycol backfilling mitigates the negative impact of the protein corona on nanoparticle cell targeting.* Angewandte Chemie International Edition, 2014. **53**(20): p. 5093-5096.

[129] Palao-Suay, R., et al., *Photothermal and photodynamic activity of polymeric nanoparticles based on α-tocopheryl succinate-RAFT block copolymers conjugated to IR-780.* Acta biomaterialia, 2017. **57**: p. 70-84.

[130] Gu, F.X., et al., *Targeted nanoparticles for cancer therapy.* Nano Today, 2007. **2**(3): p. 14-21.

[131] Broadwater, D., et al., *Modulating cellular cytotoxicity and phototoxicity of fluorescent organic salts through counterion pairing.* Scientific Reports, 2019. **9**(1): p. 15288.

[132] Sneader, W., *History of Sulfonamides.* e LS, 2001.

[133] Gaynes, R., *The Discovery of Penicillin—New Insights After More Than 75 Years of Clinical Use.* Emerging Infectious Diseases, 2017. **23**(5): p. 849-853.

[134] Woodruff, H.B., *Selman A. Waksman, winner of the 1952 Nobel Prize for physiology or medicine.* Applied and environmental microbiology, 2014. **80**(1): p. 2-8.

[135] Davies, J., *Microbes have the last word: A drastic re-evaluation of antimicrobial treatment is needed to overcome the threat of antibiotic-resistant bacteria.* EMBO reports, 2007. **8**(7): p. 616-621.

[136] Durand, G.A., D. Raoult, and G. Dubourg, *Antibiotic discovery: history, methods and perspectives.* International Journal of Antimicrobial Agents, 2019. **53**(4): p. 371-382.

[137] Llor, C. and L. Bjerrum, *Antimicrobial resistance: risk associated with antibiotic overuse and initiatives to reduce the problem.* Therapeutic advances in drug safety, 2014. **5**(6): p. 229-241.

[138] Shallcross, L.J. and D.S.C. Davies, *Antibiotic overuse: a key driver of antimicrobial resistance*. 2014, British Journal of General Practice.

[139] Zaman, S.B., et al., *A Review on Antibiotic Resistance: Alarm Bells are Ringing.* Cureus, 2017. **9**(6): p. e1403-e1403.

[140] Liu, F. and A.G. Myers, *Development of a platform for the discovery and practical synthesis of new tetracycline antibiotics.* Current Opinion in Chemical Biology, 2016. **32**: p. 48-57.

[141] Bekri, S., et al., *New antibacterial cadiolide analogues active against antibiotic-resistant strains.* Bioorganic & Medicinal Chemistry Letters, 2020. **30**(21): p. 127580.

[142] Dorst, A., et al., *Semisynthetic Analogs of the Antibiotic Fidaxomicin—Design, Synthesis, and Biological Evaluation.* ACS Medicinal Chemistry Letters, 2020.

[143] Florindo, C., et al., *Evaluation of solubility and partition properties of ampicillin-based ionic liquids.* International Journal of Pharmaceutics, 2013. **456**(2): p. 553-559.

[144] Florindo, C., et al., *Novel organic salts based on fluoroquinolone drugs: Synthesis, bioavailability and toxicological profiles.* International Journal of Pharmaceutics, 2014. **469**(1): p. 179-189.

[145] Santos, M.M., et al., *Antimicrobial Activities of Highly Bioavailable Organic Salts and Ionic Liquids from Fluoroquinolones.* Pharmaceutics, 2020. **12**(8): p. 694.

[146] Frizzo, C.P., et al., *Novel ibuprofenate- and docusate-based ionic liquids: emergence of antimicrobial activity.* RSC Advances, 2016. **6**(102): p. 100476-100486.

[147] Ferraz, R., et al., *Synthesis and Antibacterial Activity of Ionic Liquids and Organic Salts based on Penicillin G and Amoxicillin hydrolysate derivatives against Resistant Bacteria.* Pharmaceutics, 2020. **12**(3): p. 221.

[148] Rangel, J.M., et al., *Epidemiology of Escherichia coli O157: H7 outbreaks, united states, 1982-2002.* Emerging infectious diseases, 2005. **11**(4): p. 603.

[149] Gobin, M., et al., *National outbreak of Shiga toxin-producing Escherichia coli O157: H7 linked to mixed salad leaves, United Kingdom, 2016.* Eurosurveillance, 2018. **23**(18): p. 17-00197.

[150] Puño-Sarmiento, J., et al., *Potentiation of Antibiotics by a Novel Antimicrobial Peptide against Shiga Toxin Producing E. coli O157: H7.* Scientific reports, 2020. **10**(1): p. 1-14.

[151] Cole, M.R., J.A. Hobden, and I.M. Warner, *Recycling antibiotics into GUMBOS: a new combination strategy to combat multi-drug-resistant bacteria.* Molecules, 2015. **20**(4): p. 6466-6487.

[152] Cole, M., J. Hobden, and I. Warner, *Recycling Antibiotics into GUMBOS: A New Combination Strategy to Combat Multi-Drug-Resistant Bacteria.* Molecules, 2015. **20**(4): p. 6466.

[153] Newman, L.M., J.S. Moran, and K.A. Workowski, *Update on the Management of Gonorrhea in Adults in the United States.* Clinical Infectious Diseases, 2007. **44**(Supplement_3): p. S84-S101.

[154] Wi, T., et al., *Antimicrobial resistance in Neisseria gonorrhoeae: global surveillance and a call for international collaborative action.* PLoS medicine, 2017. **14**(7): p. e1002344.

[155] Lahra, M.M., et al., *Cooperative recognition of internationally disseminated ceftriaxone-resistant Neisseria gonorrhoeae strain.* Emerging infectious diseases, 2018. **24**(4): p. 735.

[156] Lopez, K.M., J.A. Hobden, and I.M. Warner, *Octenidine/carbenicillin GUMBOS as potential treatment for oropharyngeal gonorrhoea.* Journal of Antimicrobial Chemotherapy, 2020.

[157] Wu, S., et al., *Counterions-mediated gold nanorods-based sensor for label-free detection of poly(ADP-ribose) polymerase-1 activity and its inhibitor.* Sensors and Actuators B: Chemical, 2018. **259**: p. 565-572.

[158] Li, H.-Y.C., Y.-H., *Reaction-Based Amine and Alcohol Gases Detection with Triazine Ionic Liquid Materials.* Molecules, 2020. **25**: p. 104.

[159] Hsu, T.-H., S.-J. Chiang, and Y.-H. Chu, *Quartz Crystal Microbalance Analysis of Diels–Alder Reactions of Alkene Gases to Functional Ionic Liquids*

on Chips. Analytical Chemistry, 2016. **88**(22): p. 10837-10841.

[160] Li, G., et al., *Cation–Anion Interaction-Directed Molecular Design Strategy for Mechanochromic Luminescence.* Advanced Functional Materials, 2014. **24**(6): p. 747-753.

[161] Taynton, P., et al., *Repairable woven carbon fiber composites with full recyclability enabled by malleable polyimine networks.* Advanced Materials, 2016. **28**(15): p. 2904-2909.

[162] Li, G., et al., *Cation–anion interaction directed dual-mode switchable mechanochromic luminescence.* Journal of Materials Chemistry C, 2017. **5**(33): p. 8527-8534.

[163] Guimarães, L.B., et al., *Highly sensitive and precise optical temperature sensors based on new luminescent Tb3+/Eu3+ tetrakis complexes with imidazolic counterions.* Materials Advances, 2020. **1**(6): p. 1988-1995.

[164] You, L., D. Zha, and E.V. Anslyn, *Recent Advances in Supramolecular Analytical Chemistry Using Optical Sensing.* Chemical Reviews, 2015. **115**(15): p. 7840-7892.

[165] Chen, C.-Y., K.-H. Li, and Y.-H. Chu, *Reaction-Based Detection of Chemical Warfare Agent Mimics with Affinity Ionic Liquids.* Analytical Chemistry, 2018. **90**(14): p. 8320-8325.

[166] Zhang, W., et al., *AIE-doped poly(ionic liquid) photonic spheres: a single sphere-based customizable sensing platform for the discrimination of multi-analytes.* Chemical Science, 2017. **8**(9): p. 6281-6289.

[167] Achyuthan, K.E., et al., *Fluorescence superquenching of conjugated polyelectrolytes: applications for biosensing and drug discovery.* Journal of Materials Chemistry, 2005. **15**(27-28): p. 2648-2656.

[168] Thomas, S.W., G.D. Joly, and T.M. Swager, *Chemical Sensors Based on Amplifying Fluorescent Conjugated Polymers.* Chemical Reviews, 2007. **107**(4): p. 1339-1386.

[169] Jones, R.M., et al., *Superquenching and Its Applications in J-Aggregated Cyanine Polymers.* Langmuir, 2001. **17**(9): p. 2568-2571.

[170] Dickson, R.M., et al., *On/off blinking and switching behaviour of single molecules of green fluorescent protein.* Nature, 1997. **388**(6640): p. 355-358.

[171] Lin, H., et al., *Collective Fluorescence Blinking in Linear J-Aggregates Assisted by Long-Distance Exciton Migration.* Nano Letters, 2010. **10**(2): p. 620-626.

[172] Reisch, A., et al., *Collective fluorescence switching of counterion-assembled dyes in polymer nanoparticles.* Nature Communications, 2014. **5**(1): p. 4089.

[173] Würthner, F., *Perylene bisimide dyes as versatile building blocks for functional supramolecular architectures.* Chemical Communications, 2004(14): p. 1564-1579.

[174] Klymchenko, A.S., et al., *Highly lipophilic fluorescent dyes in nano-emulsions: towards bright non-leaking nano-droplets.* RSC Advances, 2012. **2**(31): p. 11876-11886.

[175] Shulov, I., et al., *Fluorinated counterion-enhanced emission of rhodamine aggregates: ultrabright nanoparticles for bioimaging and light-harvesting.* Nanoscale, 2015. **7**(43): p. 18198-18210.

[176] Andreiuk, B., et al., *An aluminium-based fluorinated counterion for enhanced encapsulation and emission of dyes in biodegradable polymer nanoparticles.* Materials Chemistry Frontiers, 2017. **1**(11): p. 2309-2316.

[177] Severi, C., N. Melnychuk, and A.S. Klymchenko, *Smartphone-assisted detection of nucleic acids by light-harvesting FRET-based nanoprobe.* Biosensors and Bioelectronics, 2020. **168**: p. 112515.

[178] Hong, S.W. and W.H. Jo, *A fluorescence resonance energy transfer probe for sensing pH in aqueous solution.* Polymer, 2008. **49**(19): p. 4180-4187.

[179] Ashokkumar, P., N. Adarsh, and A.S. Klymchenko, *Ratiometric Nanoparticle Probe Based on FRET-Amplified Phosphorescence for Oxygen Sensing with Minimal Phototoxicity.* Small, 2020. **16**(32): p. 2002494.

[180] Stoeva, S.I., et al., *Multiplexed Detection of Protein Cancer Markers with Biobarcoded Nanoparticle Probes.* Journal of the American Chemical Society, 2006. **128**(26): p. 8378-8379.

[181] Kumar, V., et al., *Nanostructured Aptamer-Functionalized Black Phosphorus Sensing Platform for Label-Free Detection of Myoglobin, a Cardiovascular Disease Biomarker.* ACS Applied Materials & Interfaces, 2016. **8**(35): p. 22860-22868.

[182] Pérez, R.L., et al., *Protein Discrimination Using a Fluorescence-Based Sensor Array of Thiacarbocyanine-GUMBOS.* ACS Sensors, 2020. **5**(8): p. 2422-2429.

[183] Hornbeck, P., *Enzyme-Linked Immunosorbent Assays.* Current Protocols in Immunology, 1992. **1**(1): p. 2.1.1-2.1.22.

[184] Ambrosi, A., F. Airò, and A. Merkoçi, *Enhanced Gold Nanoparticle Based ELISA for a Breast Cancer Biomarker.* Analytical Chemistry, 2010. **82**(3): p. 1151-1156.

[185] Pandey, S., *Analytical applications of room-temperature ionic liquids: A review of recent efforts.* Analytica Chimica Acta, 2006. **556**(1): p. 38-45.

[186] Goubaidoulline, I., G. Vidrich, and D. Johannsmann, *Organic Vapor Sensing with Ionic Liquids Entrapped in Alumina Nanopores on Quartz Crystal Resonators.* Analytical Chemistry, 2005. **77**(2): p. 615-619.

[187] Gebicki, J., *Application of ionic liquids in electronic nose instruments*, in *Analytical Applications of Ionic Liquids*. 2016, WORLD SCIENTIFIC (EUROPE). p. 339-360.

[188] Park, C.H., et al., *Ionic Liquid-Carbon Nanotube Sensor Arrays for Human Breath Related Volatile Organic Compounds.* ACS Sensors, 2018. **3**(11): p. 2432-2437.

[189] Vaughan, S.R.P., R.L.; Chhotaray, P.; Warner, I.M., *Quartz Crystal Microbalance Based Sensor Arrays for Detection and Discrimination of VOCs Using Phosphonium Ionic Liquid Composites.* Sensors and Actuators B: Chemical, 2020. **20**: p. 615.

[190] Eritt, M., et al., *OLED manufacturing for large area lighting applications.* Thin Solid Films, 2010. **518**(11): p. 3042-3045.

[191] Evans, O.R. and W. Lin, *Crystal Engineering of NLO Materials Based on Metal–Organic Coordination Networks.* Accounts of Chemical Research, 2002. **35**(7): p. 511-522.

[192] Moorthy, J.N., et al., *De Novo Design for Functional Amorphous Materials: Synthesis and Thermal and Light-Emitting Properties of Twisted Anthracene-Functionalized Bimesitylenes.* Journal of the American Chemical Society, 2008. **130**(51): p. 17320-17333.

[193] Jeong, E.G., et al., *A review of highly reliable flexible encapsulation technologies towards rollable and foldable OLEDs.* Journal of Information Display, 2020. **21**(1): p. 19-32.

[194] Justin Thomas, K.R., et al., *Light-Emitting Carbazole Derivatives: Potential Electroluminescent Materials.* Journal of the American Chemical Society, 2001. **123**(38): p. 9404-9411.

[195] Ma, D., Y. Qiu, and L. Duan, *New Insights into Tunable Volatility of Ionic Materials through Counter-Ion Control*. Advanced Functional Materials, 2016. **26**(20): p. 3438-3445.

[196] Baldo, M.A., et al., *Highly efficient phosphorescent emission from organic electroluminescent devices.* Nature, 1998. **395**(6698): p. 151-154.

[197] Thejo Kalyani, N. and S.J. Dhoble, *Organic light emitting diodes: Energy saving lighting technology—A review.* Renewable and Sustainable Energy Reviews, 2012. **16**(5): p. 2696-2723.

[198] Ma, D., L. Duan, and Y. Qiu, *Orange-red- and white-emitting diodes fabricated by vacuum evaporation deposition of sublimable cationic iridium complexes.* Journal of Materials Chemistry C, 2016. **4**(22): p. 5051-5058.

[199] Bai, R., et al., *Sky-blue-emitting cationic iridium complexes with oxadiazole/triazine-type counter-anions and their use for efficient solution-processed organic light-emitting diodes.* Dyes and Pigments, 2021. **184**: p. 108586.

[200] Tang, F., et al., *A sky-blue fluorescent small molecule for non-doped OLED using solution-processing.* RSC Advances, 2015. **5**(87): p. 71419-71424.

[201] Merklein, L.D., D.; Braig, F.; Schlisske, S.; Rödlmeier, T.; Mink, M.; Kourkoulos, D.; Ulber, B.; Di Biase, M.; Meerholz, K.; Hernandez-Sosa, G.; Lemmer, U.; Sauer, H.M.; Dörsam, E.; Scharfer, P.; Schabel, W., *Comparative Study of Printed Multilayer OLED Fabrication through Slot Die Coating, Gravure and Inkjet Printing, and Their Combination*. Colloids Interfaces, 2019. **3**: p. 32.

[202] Zhou, L., et al., *Inkjet-Printed Small-Molecule Organic Light-Emitting Diodes: Halogen-Free Inks, Printing Optimization, and Large-Area Patterning.* ACS Applied Materials & Interfaces, 2017. **9**(46): p. 40533-40540.

[203] Guo, F., et al., *The fabrication of color-tunable organic light-emitting diode displays via solution processing.* Light: Science & Applications, 2017. **6**(11): p. e17094-e17094.

[204] Chiba, T., Y.-J. Pu, and J. Kido, *Solution-processable electron injection materials for organic light-emitting devices.* Journal of Materials Chemistry C, 2015. **3**(44): p. 11567-11576.

[205] Zhang, G., et al., *Anion-controlled dimer distance induced unique solid-state fluorescence of cyano substituted styrene pyridinium*. Scientific Reports, 2016. **6**(1): p. 37609.

[206] Cosa, G., et al., *Photophysical Properties of Fluorescent DNA-dyes Bound to Single- and Double-stranded DNA in Aqueous Buffered Solution¶*. Photochemistry and Photobiology, 2001. **73**(6): p. 585-599.

[207] De Silva, T.P.D., et al., *Pyrenylpyridines: Sky-Blue Emitters for Organic Light-Emitting Diodes.* ACS Omega, 2019. **4**(16): p. 16867-16877.

[208] Cole, J.M., et al., *Cosensitization in Dye-Sensitized Solar Cells.* Chemical Reviews, 2019. **119**(12): p. 7279-7327.

[209] Pagliaro, M., R. Ciriminna, and G. Palmisano, *BIPV: merging the photovoltaic with the construction industry.* Progress in Photovoltaics: Research and Applications, 2010. **18**(1): p. 61-72.

[210] Zhang, K., et al., *High-Performance, Transparent, Dye-Sensitized Solar Cells for See-Through Photovoltaic Windows.* Advanced Energy Materials, 2014. **4**(11): p. 1301966.

[211] Mohamad, A.A., *Physical properties of quasi-solid-state polymer electrolytes for dye-sensitised solar cells: A characterisation review.* Solar Energy, 2019. **190**: p. 434-452.

[212] Kuang, D., et al., *High Molar Extinction Coefficient Ion-Coordinating Ruthenium Sensitizer for Efficient and Stable Mesoscopic Dye-Sensitized Solar Cells.* Advanced Functional Materials, 2007. **17**(1): p. 154-160.

[213] Wang, P., et al., *A stable quasi-solid-state dye-sensitized solar cell with an amphiphilic ruthenium sensitizer and polymer gel electrolyte.* Nature Materials, 2003. **2**(6): p. 402-407.

[214] Abbotto, A., et al., *Panchromatic ruthenium sensitizer based on electron-rich heteroarylvinylene π-conjugated quaterpyridine for dye-sensitized solar cells.* Dalton Transactions, 2011. **40**(1): p. 234-242.

[215] Jradi, F.M., et al., *Near-Infrared Asymmetrical Squaraine Sensitizers for Highly Efficient Dye Sensitized Solar Cells: The Effect of π-Bridges and Anchoring Groups on Solar Cell Performance.* Chemistry of Materials, 2015. **27**(7): p. 2480-2487.

[216] Saccone, D., et al., *Polymethine Dyes in Hybrid Photovoltaics: Structure–Properties Relationships.* European Journal of Organic Chemistry, 2016. **2016**(13): p. 2244-2259.

[217] Osedach, T.P., et al., *Near-infrared photodetector consisting of J-aggregating cyanine dye and metal oxide thin films.* Applied Physics Letters, 2012. **101**(11): p. 113303.

[218] Hales, J.M., et al., *Design of Polymethine Dyes with Large Third-Order Optical Nonlinearities and Loss Figures of Merit.* Science, 2010. **327**(5972): p. 1485.

[219] Zhao, Y., et al., *Near-Infrared Harvesting Transparent Luminescent Solar Concentrators.* Advanced Optical Materials, 2014. **2**(7): p. 606-611.

[220] Fan, B., et al., *High performing doped cyanine bilayer solar cell.* Organic Electronics, 2010. **11**(4): p. 583-588.

[221] Eskandari, M., et al., *Counterion-Mediated Crossing of the Cyanine Limit in Crystals and Fluid Solution: Bond Length Alternation and Spectral Broadening Unveiled by Quantum Chemistry.* Journal of the American Chemical Society, 2020. **142**(6): p. 2835-2843.

[222] Gayton, J.N.A., S.; Fortenberry, R.C.; Hammer, N.I.; Delcamp, J.H., *Counter Anion Effect on the Photophysical Properties of Emissive Indolizine-Cyanine Dyes in Solution and Solid State.* Molecules, 2018. **23**: p. 3051.

[223] Huckaba, A.J., et al., *A low recombination rate indolizine sensitizer for dye-sensitized solar cells.* Chemical Communications, 2016. **52**(54): p. 8424-8427.

[224] Glinka, A., et al., *Interface Modification and Exceptionally Fast Regeneration in Copper Mediated Solar Cells Sensitized with Indoline Dyes.* The Journal of Physical Chemistry C, 2020. **124**(5): p. 2895-2906.

[225] Abu Talip, R.A.Y., W.Z.N.; Bustam, M.A, *Ionic Liquids Roles and Perspectives in Electrolyte for Dye-Sensitized Solar Cells.* Sustainability, 2020. **12**: p. 7598.

[226] Bahadar Khan, S., et al., *Photovoltaic Performance of Porphyrin-Based Dye-Sensitized Solar Cells with Binary Ionic Liquid Electrolytes.* Energy Technology, 2020. **8**(6): p. 2000092.

[227] Cao, Y., et al., *11% efficiency solid-state dye-sensitized solar cells with copper(II/I) hole transport materials.* Nature Communications, 2017. **8**(1): p. 15390.

[228] Ravi, S.K., et al., *Optical manipulation of work function contrasts on metal thin films.* Science Advances, 2018. **4**(3): p. eaao6050.

[229] Naghdi, S., G. Sanchez-Arriaga, and K.Y. Rhee, *Tuning the work function of graphene toward application as anode and cathode.* Journal of Alloys and Compounds, 2019. **805**: p. 1117-1134.

[230] Peng, X., et al., *Low Work Function Surface Modifiers for Solution-Processed Electronics: A Review.* Advanced Materials Interfaces, 2018. **5**(10): p. 1701404.

[231] Zhou, Y., et al., *A Universal Method to Produce Low–Work Function Electrodes for Organic Electronics.* Science, 2012. **336**(6079): p. 327.

[232] Ohisa, S., et al., *Doping of Tetraalkylammonium Salts in Polyethylenimine Ethoxylated for Efficient Electron Injection Layers in Solution-Processed Organic Light-Emitting Devices.* ACS Applied Materials & Interfaces, 2019. **11**(28): p. 25351-25357.

[233] Duan, J., et al., *Cationic Polyelectrolytes with Alkylsulfonate Counterions as a Cathode Interface Layer for High-Performance Polymer Solar Cells.* ACS Applied Materials & Interfaces, 2020.